

Scalar leptoquarks at the LHC and flavour anomalies: a comparison of pair-production modes at NLO-QCD

Christoph Borschensky^a, Benjamin Fuks^b, Adil Jueid^c and Anna Kulesza^{d,e}

^a*Institut für Theoretische Physik, Karlsruhe Institute for Technology, 76128 Karlsruhe, Germany*

^b*Laboratoire de Physique Théorique et Hautes Énergies (LPHE), UMR 7589, Sorbonne Université et CNRS, 4 place Jussieu, 75252 Paris Cedex 05, France*

^c*Quantum Universe Center, Korea Institute for Advanced Study, Seoul 02455, Republic of Korea*

^d*Institut für Theoretische Physik, WWU Münster, D-48149 Münster, Germany*

^e*Theoretical Physics Department, CERN, 1211 Geneva 23, Switzerland*

E-mail: christoph.borschensky@kit.edu, fuks@lpthe.jussieu.fr,
adiljueid@kias.re.kr, anna.kulesza@uni-muenster.de

ABSTRACT: We analyse scalar leptoquark pair production at the LHC with predictions including t -channel lepton exchange contributions up to next-to-leading order (NLO) in QCD. In particular, we calculate NLO-QCD predictions for off-diagonal production channels, *i.e.* channels that involve two different leptoquark eigenstates and are driven solely by diagrams involving Standard Model leptons in the t -channel at leading order, as opposed to diagonal channels where a pair of the same leptoquark eigenstate is produced. We find that reliable theoretical predictions for both channels require NLO accuracy. The relative importance of the off-diagonal modes depends strongly on the considered scenario. In a generic model involving R_2 and S_3 leptoquarks, at large values of the Yukawa couplings off-diagonal contributions initiated by valence quarks can be up to an order of magnitude higher than the diagonal production. However, we also find that in phenomenologically viable scenarios addressing the flavour anomalies off-diagonal production is generally negligible, with a few exceptions of 10%–30% of the total rate depending on the treatment of the charm density in the proton.

Contents

1	Introduction	1
2	Theoretical setup	3
2.1	Phenomenological leptoquark models	3
2.2	Benchmark scenarios	4
2.2.1	General scenarios including R_2 and S_3 leptoquarks coupling to first- and second-generation quarks	5
2.2.2	Benchmark scenarios addressing the flavour anomalies	6
2.3	Leptoquark pair production at next-to-leading order	7
3	Scalar leptoquark pair production in general scenarios	9
3.1	Technical setup	9
3.2	NLO cross sections in the R_2 – S_3 model	9
3.3	t -channel and off-diagonal contributions on inclusive leptoquark production rates in the R_2 – S_3 model	13
4	Role of the off-diagonal production modes in scenarios addressing the flavour anomalies	18
4.1	Total cross sections at NLO	18
4.2	Impact of the charm PDF on the predictions	21
5	Conclusions	22
A	Leading-order amplitudes for off-diagonal leptoquark pair production	23
B	Additional results for $m_{LQ} = 2400$ GeV	25

1 Introduction

Scalar leptoquarks are scalar bosons beyond the Standard Model which carry both lepton and baryon numbers, and therefore couple simultaneously to leptons and quarks via a Yukawa-type interaction. Originally proposed in models of Grand Unification [1–7], they appear in many extensions to the Standard Model, *e.g.* in superstring models [8], R -parity violating supersymmetric scenarios [9, 10], composite models [11–15], neutrino mass models [16–21], or as mediators in simplified models of dark matter [22–27]. Scalar leptoquarks may also offer an explanation [28–35] to the anomalies appearing in B -physics

observables [36–43], as well as to the discrepancy between theoretical predictions [44] and experimental measurements [45, 46] related to the anomalous magnetic moment of the muon. In this context, most interesting scenarios feature large Yukawa couplings between leptons, quarks, and leptoquarks.

The ATLAS and CMS collaborations at the Large Hadron Collider (LHC) have so far measured no signals hinting at the existence of scalar leptoquarks, thus pushing the mass limits of first, second, and third generation leptoquarks up to around 1.0–1.8 TeV [47–54], depending on the considered leptoquark model and benchmark scenario. The most stringent limits originate from LHC direct searches for the pair production of scalar leptoquarks, assuming that the Yukawa couplings are small so that the production is driven purely by QCD interactions. This assumption is clearly at odds with possible explanations of lepton flavour anomalies. Consequently, Yukawa coupling-induced contributions ought to be included in studies of leptoquark production at the LHC.

From the theoretical side, calculations for cross sections of scalar leptoquark pair production are available at the next-to-leading order (NLO) in the strong coupling constant α_s already for some time [55, 56]. More recently these fixed-order calculations have been matched with parton showers [57, 58], and with soft-gluon resummation up to next-to-next-to-leading logarithmic accuracy [59–61]. In the latter works, in addition to the pure-QCD contribution, also so-called t -channel contributions (*i.e.* diagrams with a t -channel lepton exchange that are proportional to the leptoquark Yukawa couplings) have been taken into account. It has been shown that for phenomenologically relevant parameter points, these additional terms can be sizeable and can interplay in an intricate way with soft-gluon corrections. Furthermore, the expected production rates turn out to depend strongly on the chosen leptoquark model and benchmark scenario, as well as on the set of parton distribution functions (PDF) used for the calculations. All these effects need thus to be considered for the best exploitation of scalar leptoquark searches.

Besides pair production of scalar leptoquarks, other relevant processes for leptoquark searches at hadron colliders include their single production in association with a lepton [62–65], Drell-Yan di-lepton production with leptoquarks appearing as virtual particles [66–72], and resonant leptoquark production through quark-lepton initial states [73–76]. Recently, a novel channel related to the pair production of scalar leptoquarks has been introduced [77]. In certain scenarios with at least two leptoquark eigenstates, there exists the possibility to produce a ‘diagonal’ pair of leptoquarks of the same eigenstate, or to ‘off-diagonally’ produce two different leptoquark states. In contrast to the diagonal production, the off-diagonal channel is, at tree level, purely driven by the strength of the leptoquark Yukawa couplings and independent of the strong coupling constant. In addition, the quark-quark channel opens up, with quarks of possibly unequal flavours. This is particularly suited for LHC studies as one can expect large cross sections if two valence quarks are involved.

For instance, it has been shown at leading order (LO) in [77] that for a one-flavour new physics realisation based on a model including both S_1 and R_2 leptoquarks, the *total* pair production rates can be enhanced strongly relative to the expectation from pure QCD production, and this even for moderate leptoquark Yukawa couplings. In addition, the off-diagonal production channels have the potential to outweigh the importance of other Yukawa-coupling-dependent search channels, especially for moderate to large Yukawa couplings.

In the present work, we investigate the relevance of the off-diagonal production mechanism in more detail, in particular in the context of models relevant for explaining flavour anomalies. Given the impact of higher-order QCD effects on the predictions for scalar leptoquark pair-production reported in [59–61], and generally their relevance for the production of heavy coloured particles in hadronic channels, we increase the precision of the off-diagonal production mechanism of scalar leptoquarks by calculating the associated NLO-QCD corrections. We also compare the off-diagonal production rates with diagonal production through both QCD and Yukawa coupling-induced t -channel mechanisms. The computations are included in our framework of scalar leptoquark pair production for various leptoquark models [59–61] with the MADGRAPH5_AMC@NLO [78] and POWHEG-BOX [79–81] software. In addition, we comprehensively study the impact of the Yukawa-coupling-driven contributions on inclusive rates for phenomenologically viable leptoquark models that offer a solution to the flavour anomalies.

The structure of this paper is as follows. In section 2, we discuss our theoretical setup and the specific benchmark leptoquark scenarios that we study, followed by a brief review of leptoquark pair production at fixed order. We then introduce some computational details in section 3, and next analyse the numerical impact of the off-diagonal production modes on total rates. In this context, we consider a general scenario including R_2 and S_3 leptoquarks coupling to quarks of the first and second generation. An application of our calculations to phenomenologically viable benchmark scenarios is subsequently presented in section 4, where we also highlight the role of the charm PDF on production rates. At last, we conclude in section 5.

2 Theoretical setup

2.1 Phenomenological leptoquark models

We consider various simplified leptoquark models where the Standard Model (SM) is supplemented by the following species of scalar leptoquarks: S_1 , R_2 , and S_3 . We furthermore assume that these leptoquarks couple only to the SM fermions and not to exotic beyond-the-SM ones. Following the notation of references [82, 83], these leptoquarks transform as $S_1 : (\mathbf{3}, \mathbf{1})_{-1/3}$, $R_2 : (\mathbf{3}, \mathbf{2})_{7/6}$, $S_3 : (\mathbf{3}, \mathbf{3})_{-1/3}$ under the $SU(3)_c \otimes SU(2)_L \otimes U(1)_Y$ gauge group.

Following these transformation rules, the most general gauge invariant and renormalisable Lagrangian involving the S_1 , R_2 , and S_3 species is given by¹

$$\begin{aligned}\mathcal{L}_{\text{LQ}} = & \mathcal{L}_{\text{kin.}} + \mathcal{L}_{\text{mass}} + \mathbf{y}_1^{\text{RR}} \bar{u}_R^c \ell_R S_1^\dagger + \mathbf{y}_1^{\text{LL}} (\bar{Q}_L^c \cdot L_L) S_1^\dagger + \mathbf{y}_2^{\text{LR}} \bar{\ell}_R Q_L R_2^\dagger \\ & + \mathbf{y}_2^{\text{RL}} \bar{u}_R (L_L \cdot R_2) + \mathbf{y}_3^{\text{LL}} (\bar{Q}_L^c \cdot \sigma_k L_L) (S_3^k)^\dagger + \text{H.c.},\end{aligned}\quad (2.1)$$

where we have represented the S_3 multiplet as a vector carrying an adjoint $SU(2)_L$ index, namely S_3^k with $k = 1, 2, 3$. An alternative way to write the above Lagrangian could make use of a matrix representation for $SU(2)_L$ triplets. In this case, $S_3 \equiv (S_3)^\alpha_{\dot{\alpha}} = \frac{1}{\sqrt{2}} (\sigma_k)^\alpha_{\dot{\alpha}} S_3^k$, where the S_3 matrix carries a fundamental ($\alpha = 1, 2$) and an antifundamental ($\dot{\alpha} = 1, 2$) index of $SU(2)_L$, and where σ_k are the usual Pauli matrices. In addition, $(\bar{Q}_L^c \cdot L_L)$, $(L_L \cdot R_2)$, $(\bar{Q}_L^c \cdot \sigma_k L_L)$ refer to standard $SU(2)_L$ invariant products. In the above Lagrangian, we have suppressed both generation as well as colour indices. All the couplings \mathbf{y} are 3×3 matrices in the flavour space and which can be complex as well. The first index of any element y_{ij} of a coupling matrix \mathbf{y} refers to a quark generation while the second index refers to a lepton generation. The quark and lepton multiplets are denoted by Q_L and L_L (quark and lepton weak isodoublets), u_R , d_R and ℓ_R (quark and lepton isosinglets). Finally, all the kinetic and mass terms involving scalar leptoquarks are encoded in $\mathcal{L}_{\text{kin.}}$ and $\mathcal{L}_{\text{mass}}$, respectively.

The scalar leptoquarks are represented as follows,

$$S_1 = S_1^{(-1/3)}, \quad R_2 = \begin{pmatrix} R_2^{(+5/3)} \\ R_2^{(+2/3)} \end{pmatrix}, \quad S_3 = \begin{pmatrix} \frac{1}{\sqrt{2}} S_3^{(-1/3)} & S_3^{(+2/3)} \\ S_3^{(-4/3)} & -\frac{1}{\sqrt{2}} S_3^{(-1/3)} \end{pmatrix}, \quad (2.2)$$

with the superscripts referring to the electric charge of the leptoquark eigenstates. Expanding the multiplets in the Lagrangian of eq. (2.1) in terms of the eigenstates of eq. (2.2), we obtain:

$$\begin{aligned}\mathcal{L}_{\text{LQ}} = & \mathcal{L}_{\text{kin.}} + \mathcal{L}_{\text{mass}} + \mathbf{y}_1^{\text{RR}} \bar{u}_R^c \ell_R S_1^{(+1/3)} + \mathbf{y}_1^{\text{LL}} (\bar{u}_L^c \ell_L S_1^{(+1/3)} - \bar{d}_L^c \nu_L S_1^{(+1/3)}) \\ & + \mathbf{y}_2^{\text{LR}} (\bar{\ell}_R u_L R_2^{(-5/3)} + \bar{\ell}_R d_L R_2^{(-2/3)}) + \mathbf{y}_2^{\text{RL}} (\bar{u}_R \nu_L R_2^{(+2/3)} - \bar{u}_R \ell_L R_2^{(+5/3)}) \\ & + \mathbf{y}_3^{\text{LL}} (\sqrt{2} \bar{u}_L^c \nu_L S_3^{(-2/3)} - \bar{u}_L^c \ell_L S_3^{(+1/3)} - \bar{d}_L^c \nu_L S_3^{(+1/3)} - \sqrt{2} \bar{d}_L^c \ell_L S_3^{(+4/3)}) \\ & + \text{H.c.}\end{aligned}\quad (2.3)$$

2.2 Benchmark scenarios

To illustrate the effect of t -channel diagrams, NLO-QCD corrections, and off-diagonal channels on scalar leptoquark pair production rates, we define below a few benchmark scenarios. We first consider generic simplified scenarios derived from models offering promising solutions to the flavour anomalies. Then we move on with an estimation of the impact of off-diagonal leptoquark production channels in the context of the phenomenologically motivated scenarios that were studied in depth in [60].

¹We do not study the scalar potential involving Higgs multiplets and scalar leptoquarks (that can be found, *e.g.*, in [84]), since we are studying scalar leptoquark pair production in simplified models.

2.2.1 General scenarios including R_2 and S_3 leptoquarks coupling to first- and second-generation quarks

We begin the present work with a study of scalar leptoquark pair production in models involving simultaneously R_2 and S_3 leptoquarks, our calculations including both diagonal and off-diagonal channels. The term *diagonal* refers here to the production of a particle-antiparticle pair of the *same* leptoquark eigenstate, while the term *off-diagonal* stands for the production of two *different* leptoquark eigenstates. Consequently, in the case of a multi-species leptoquark model, the off-diagonal production mode does not only include the production of two different leptoquark states from a given multiplet, but also that of eigenstates of different multiplets.

To simplify the discussion and the physics analysis performed in our adopted R_2 – S_3 model, we assume a mass degeneracy among all leptoquark states considered, and we compute the cross sections for two leptoquark masses²,

$$m_{\text{LQ}} \equiv m_{R_2} = m_{S_3} = 1600 \text{ GeV} \quad \text{and} \quad 2400 \text{ GeV}. \quad (2.4)$$

In this scenario, off-diagonal leptoquark production includes seven channels. In order to make the discussion as generic as possible, we set all the relevant entries of the Yukawa coupling matrices to zero except $y_{2,12}^{\text{LR}}$, $y_{2,12}^{\text{RL}}$, and $y_{3,12}^{\text{LL}}$. Furthermore, we assume a degeneracy among these couplings, and let them vary over the following range,

$$y \equiv y_{2,12}^{\text{LR}} = y_{2,12}^{\text{RL}} = y_{3,12}^{\text{LL}} \in [0.1, 1.5]. \quad (2.5)$$

Processes involving different leptoquark species hence depend on the product of two of the couplings of eq. (2.5), which eventually leads to a y^4 dependence of the tree-level cross section. In appendix A, we detail how these different couplings lead to the opening of the different off-diagonal production modes, and how the associated cross sections are related to each other.

In another scenario, we ignore the contributions of the S_3 leptoquark and analyse a model containing only R_2 leptoquarks. We consider a dependence on the Yukawa couplings in two configurations: (i) couplings to first-generation quarks only and (ii) couplings to second-generation quarks only,

$$\begin{aligned} (i): \quad & y_{2,12}^{\text{LR}} \in [0.1, 1.5], \quad y_{2,22}^{\text{LR}} = 0, \\ (ii): \quad & y_{2,22}^{\text{LR}} \in [0.1, 1.5], \quad y_{2,12}^{\text{LR}} = 0. \end{aligned} \quad (2.6)$$

We set in both cases all other couplings to zero, and in particular $y_{2,12}^{\text{RL}} = y_{2,22}^{\text{RL}} = 0$.

²Whereas our lowest mass choice may be excluded by recent ATLAS results [49] that suggest a lower mass limit of 1.7–1.8 TeV on scalar leptoquarks coupling to muons and electrons, production characteristics are not drastically affected by the actual mass value in this range.

	$y_{2,23}^{\text{RL}}$	$y_{2,33}^{\text{LR}}$	$y_{2,21}^{\text{LR}}$	$y_{2,31}^{\text{LR}}$
a_1	$1.84 + 1.84i$	$0.354 + 0.354i$	$-0.015i$	$0.262 + 0.262i$
a_2	$0.309 + 0.951i$	$0.951 + 0.309i$	$0.011 - 0.011i$	$0.37i$

Table 1. Non-zero Yukawa couplings for two benchmark points in a model that includes a single R_2 leptoquark species (with a mass of 1 TeV), and that provides an explanation for the flavour anomalies according to [85]. The two points have been selected from the 1σ ranges of model parameters allowing to explain the anomalies.

	$y_{2,33}^{\text{LR}}$	$y_{2,22}^{\text{RL}}$	$y_{2,23}^{\text{RL}}$	$y_{3,22}^{\text{LL}}$	$y_{3,23}^{\text{LL}}$	$y_{3,32}^{\text{LL}}$	$y_{3,33}^{\text{LL}}$
b_1	$-0.18734 + 1.12287i$	0.265001	1.17382	-0.010	-0.045	-0.265	-1.173
b_2	$-0.18734 + 1.12287i$	0.37353	1.59511	-0.014	-0.061	-0.373	-1.594

Table 2. Non-zero Yukawa couplings for two benchmark points in a two-leptoquark model allowing for an explanation for the flavour anomalies [86, 87]. Benchmarks include an R_2 leptoquark (with $m_{R_2} = 1.3$ TeV) and an S_3 leptoquark (with $m_{S_3} = 2$ TeV). Point b_1 corresponds to the best fit value and b_2 is chosen inside the 2σ region returned by the fit.

2.2.2 Benchmark scenarios addressing the flavour anomalies

Phenomenologically-viable R_2 models – An interesting scenario that minimally addresses all flavour anomalies with a unique species of scalar leptoquarks has been suggested in [85]. In that scenario, the SM is extended by a single leptoquark doublet R_2 that couples to tau leptons and to electrons, which is sufficient to address both the $R_{D^{(*)}}$ and the $R_{K^{(*)}}$ anomalies. In this context and based on the results of [85], we consider two benchmark points denoted by a_1 and a_2 with $m_{R_2} = 1000$ GeV (see table 1). Whereas these choices lead to mild tensions between data and theory for the $\text{BR}(B_c \rightarrow \tau\nu)$ branching ratio, these can be weakened by considering non-minimal models involving two leptoquark species, like R_2 and S_3 .

A two-leptoquark R_2 – S_3 model inspired by Grand Unification – Here, the SM is extended by several leptoquark species with masses lying in the TeV regime. Such a model was proposed in [86], where it was shown that the presence of two leptoquarks R_2 and S_3 suffices to address the $R_{D^{(*)}}$ and $R_{K^{(*)}}$ anomalies and to avoid all constraints from direct and indirect searches for leptoquarks at the LHC, from LEP-I precision measurements at the Z -pole, and from measurements of other flavour observables. Following the updated fit of [87], we consider two scenarios dubbed b_1 and b_2 with $m_{R_2} = 1300$ GeV and $m_{S_3} = 2000$ GeV (see table 2).

	$y_{1,22}^{\text{LL}}$	$y_{1,23}^{\text{LL}}$	$y_{1,32}^{\text{LL}}$	$y_{1,33}^{\text{LL}}$	$y_{1,23}^{\text{RR}}$	$y_{1,32}^{\text{RR}}$	$y_{3,22}^{\text{LL}}$	$y_{3,23}^{\text{LL}}$	$y_{3,32}^{\text{LL}}$	$y_{3,33}^{\text{LL}}$
c_1	-0.0082	-1.46	-0.016	-0.064	1.34	-0.19	-0.019	0.58	-0.059	-0.11
c_2	0.0078	1.36	-0.055	0.052	-1.47	-0.053	-0.017	-1.23	-0.070	0.066

Table 3. Non-zero Yukawa couplings for two benchmark points in a two-leptoquark scenario providing an explanation for the flavour anomalies [88]. Benchmarks include S_1 and S_3 leptoquarks (with $m_{\text{LQ}} = 1.2 \text{ TeV}$). Points c_1 and c_2 correspond to the p_1 and p_2 benchmarks in the notation of [88].

The singlet-triplet S_1 – S_3 leptoquark model – Ref. [88] demonstrated that a possible solution to the flavour anomalies could be designed by extending the SM by two leptoquark species S_1 and S_3 , provided that the leptoquarks couple to muons and tau leptons. In addition, this framework reduces the gap between the theory prediction and the experimental measurement of the anomalous magnetic moment of the muon. We use two benchmark points c_1 and c_2 , that correspond to the p_1 and p_2 setups from [88], in which we choose leptoquark masses $m_{S_1} = m_{S_3} = 1200 \text{ TeV}$. Details about these benchmarks can be found in table 3.

2.3 Leptoquark pair production at next-to-leading order

We discuss in this section general features of scalar leptoquark pair production in proton-proton collisions. We consider the following process

$$pp \rightarrow \text{LQ}_i \text{LQ}_j + X, \quad (2.7)$$

where LQ_i and LQ_j refer generically to any (possibly identical) leptoquark species. In the following, we always sum over charge-conjugate processes when they are different. For instance, $pp \rightarrow S_3^{(\pm 1/3)} S_3^{(\pm 2/3)}$ would refer to both the production of an $S_3^{(+1/3)} S_3^{(+2/3)}$ and an $S_3^{(-1/3)} S_3^{(-2/3)}$ pair. The corresponding NLO total production rate is given by

$$\sigma_{\text{NLO}} = \sum_{a,b=q,\bar{q},g} \int dx_a dx_b f_{a/p}(x_a, \mu_F^2) f_{b/p}(x_b, \mu_F^2) \hat{\sigma}_{\text{NLO}}(ab \rightarrow \text{LQ}_i \text{LQ}_j), \quad (2.8)$$

where x_i stands for the momentum fraction of the parton i inside the proton, $f_{i/p}$ for its parton distribution function evaluated at a factorisation scale μ_F , and $\hat{\sigma}$ is the (NLO-QCD) partonic cross section. It includes Born contributions $\sigma^{(0)}$ and $\mathcal{O}(\alpha_s)$ corrections $\sigma^{(1)}$ for both of which a selection of Feynman diagrams is shown in figure 1, in the diagonal and off-diagonal case.

For the diagonal channel, the Born component of the cross section receives pure QCD contributions that are proportional to α_s^2 [diagrams (a1)–(a4)], t -channel lepton exchange contributions that are proportional to y^4 [diagram (a5)], and the interference between

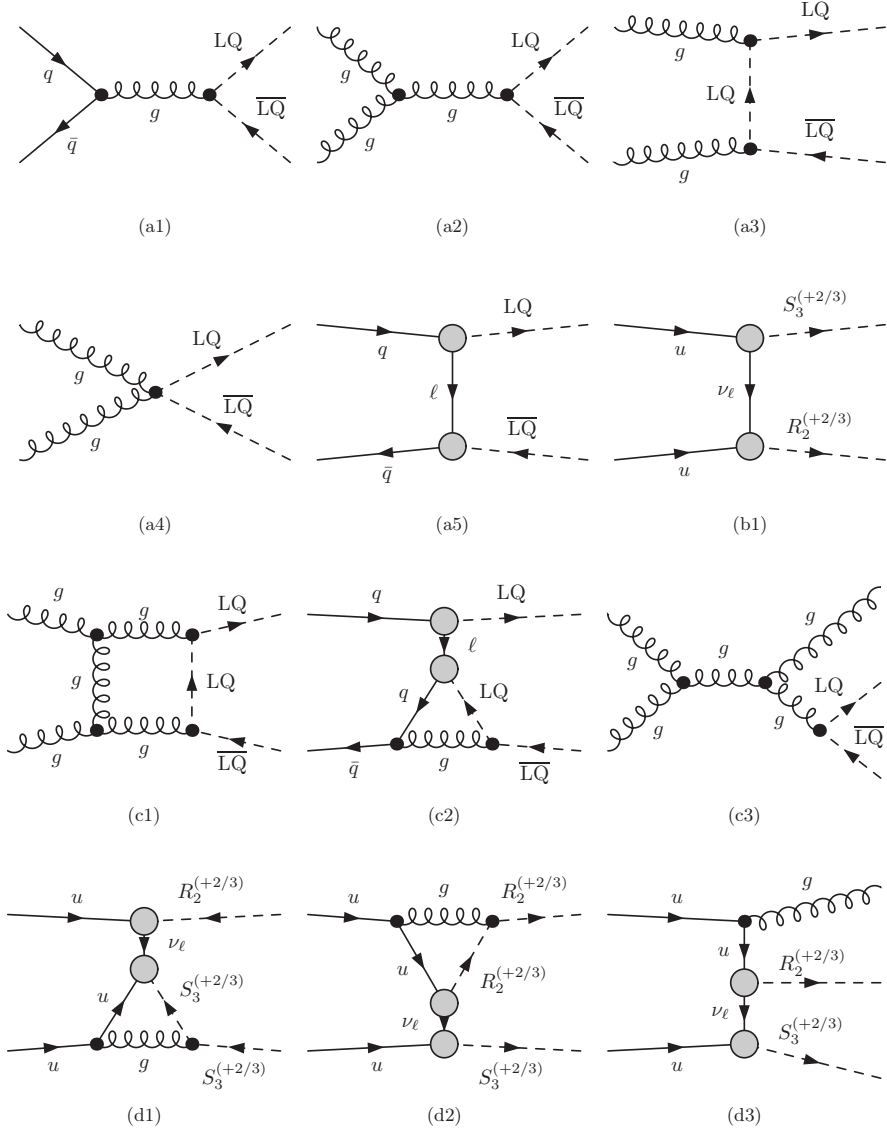


Figure 1. Selection of Feynman diagrams contributing to scalar leptoquark pair production in hadron collisions, both for the diagonal and off-diagonal channel (for which we have chosen the $pp \rightarrow R_2^{(+2/3)} S_3^{(+2/3)}$ example). QCD couplings are indicated by a black point, while a grey circle denotes the lepton-quark-leptoquark Yukawa couplings. Born diagrams are shown in the sub-panels (a1)–(a5) for the diagonal case, and (b1) for the off-diagonal one. Virtual correction and real emission diagrams are shown in sub-panels (c1)–(c3) and (d1)–(d3) respectively.

the two that is of $\mathcal{O}(\alpha_s y^2)$. In contrast, only t -channel exchange diagrams survive for off-diagonal leptoquark pair production modes [diagram (b1)]. NLO corrections to the diagonal case therefore include three classes of contributions, namely one proportional to α_s^3 (the pure QCD component of $\sigma^{(1)}$), one proportional to $\alpha_s y^4$ (NLO-QCD corrections to t -channel exchange contributions) and one proportional to $\alpha_s^2 y^2$ (NLO-QCD corrections

to the interference between QCD and t -channel amplitudes). In the off-diagonal case, only $\mathcal{O}(\alpha_s y^4)$ contributions are obviously relevant. Correspondingly, diagrams (c1)–(c2) and (d1)–(d2) illustrate virtual loop corrections, whereas diagrams (c3) and (d3) are examples of real-emission corrections.

3 Scalar leptoquark pair production in general scenarios

3.1 Technical setup

Calculations of fixed-order cross sections at LO and NLO are performed using MADGRAPH_AMC@NLO version 3.1.1 [78] and the LQnlo_5FNS_v5 UFO [89] model documented in [59, 60]³. To assess the dependence of the results on the PDF choice, we use two LO and three NLO PDF sets accessed through LHAPDF 6.4.0 [90]: MSHT20lo_as_130 [91] (with $\alpha_s(M_Z) = 0.130$), NNPDF40_lo_as_01180 [92], MSHT20nlo_as_118 [91], CT18NLO [93] and NNPDF40_nlo_as_01180 [92] (all four last sets using $\alpha_s(M_Z) = 0.118$). Moreover, we fix the renormalisation and the factorisation scale to the mass of the produced scalar leptoquarks $\mu_R = \mu_F = m_{LQ}$, and estimate scale uncertainties with the seven-point method (in which the error is computed from the envelope spanned by the cross section when varying the scales independently by a factor of 2 up and down, while keeping their ratio to at most 2).

In order to validate our predictions, we compute independently cross sections using the POWHEG-BOX v2 framework [79–81]. Here, the relevant virtual amplitudes have been generated with FEYNARTS [94] and FORMCALC [95], and are based on a manual implementation of the leptoquark interaction vertices in an *ad hoc* FEYNARTS model. We have found excellent agreement between the MADGRAPH5_AMC@NLO and POWHEG-BOX predictions.

Technical details about the necessary modifications of the MADGRAPH5_AMC@NLO and POWHEG-BOX packages to compute leptoquark production rates and about how to run the codes can be found in [60].

3.2 NLO cross sections in the R_2 – S_3 model

We focus first in figure 2 on total cross sections for the production of leptoquarks of the R_2 species, the leptoquark mass being fixed to 1600 GeV. While the plots on the left and in the middle panels of the figure present results for the two diagonal production modes, *i.e.* for the production of $R_2^{(+2/3)} R_2^{(-2/3)}$ and $R_2^{(+5/3)} R_2^{(-5/3)}$ leptoquark pairs, the plot on the right of the figure concerns the off-diagonal production of an $R_2^{(\pm 2/3)} R_2^{(\mp 5/3)}$ pair of leptoquarks (the contributions of the two conjugate processes being summed over). In the former case, the leptoquark Yukawa coupling y impacts the NLO rates only for values larger than $y \sim 0.6$, the pure QCD channel being largely dominant for smaller y values. In contrast,

³The model is available from <https://www.uni-muenster.de/Physik.TP/research/kulesza/leptoquarks.html>.

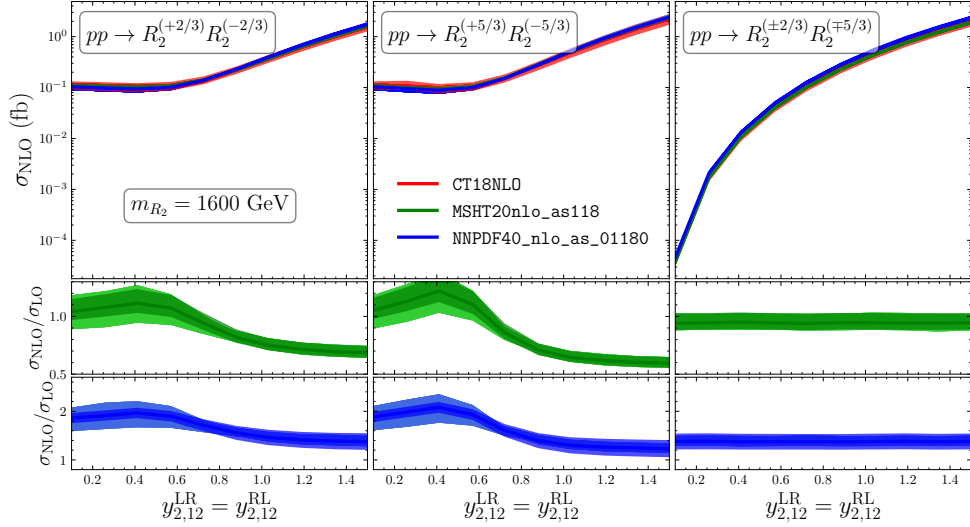


Figure 2. Total cross sections for the production of a pair of R_2 eigenstates as a function of $y = y_{2,12}^{\text{LR}} = y_{2,12}^{\text{RL}}$ for the three processes $pp \rightarrow R_2^{(+2/3)} R_2^{(-2/3)}$ (left), $pp \rightarrow R_2^{(+5/3)} R_2^{(-5/3)}$ (middle) and $pp \rightarrow R_2^{(\pm 5/3)} R_2^{(\mp 2/3)}$ (right). In the lower panels, we present NLO K -factors defined as the ratio of the NLO rates to the LO ones for the MSHT20 and CT18 PDF sets. Our predictions include scale (light error bands) and PDF (darker error bands) uncertainties at NLO (evaluated relatively to the central LO predictions for the K -factors).

the off-diagonal channel only involves diagrams depending on the Yukawa coupling y , so that the corresponding cross section is negligible for small values of y and grows steadily with the coupling. At larger values of y , it delivers a comparable contribution to that of the diagonal mode with t -channel exchange included.

In addition, we compare total rate predictions obtained with the MSHT20nlo_as_118 (green), CT18NLO (red) and NNPDF40_nlo_as_01180 (blue) sets of parton densities in the upper panel of the figure. In the lower panel we show K -factors defined as the ratio of the NLO rates to the LO ones when MSHT20 and NNPDF4.0 densities are used, LO rates being respectively evaluated with the MSHT20lo_as_130 and NNPDF40_lo_as_01180 PDF sets⁴. Whereas all NLO cross sections are found to agree within their uncertainties, the values of the K -factors strongly depend on the used PDF set, as visible from the lower panels of figure 2. This behaviour originates from strong differences inherent to the LO PDF sets, which emphasises that NLO predictions are mandatory for reliable results. Moreover, for all channels and all choices of parton densities, NLO corrections are significant. Their effects are found to modify LO rates by a value ranging from tens of percents to up to a factor of 2, the exact value depending on y and the PDF set.

The shape of the K -factors as a function of the Yukawa coupling y is found to be similar

⁴ K -factors associated with CT18 densities have not been computed as the CT18 LO set is not publicly available.

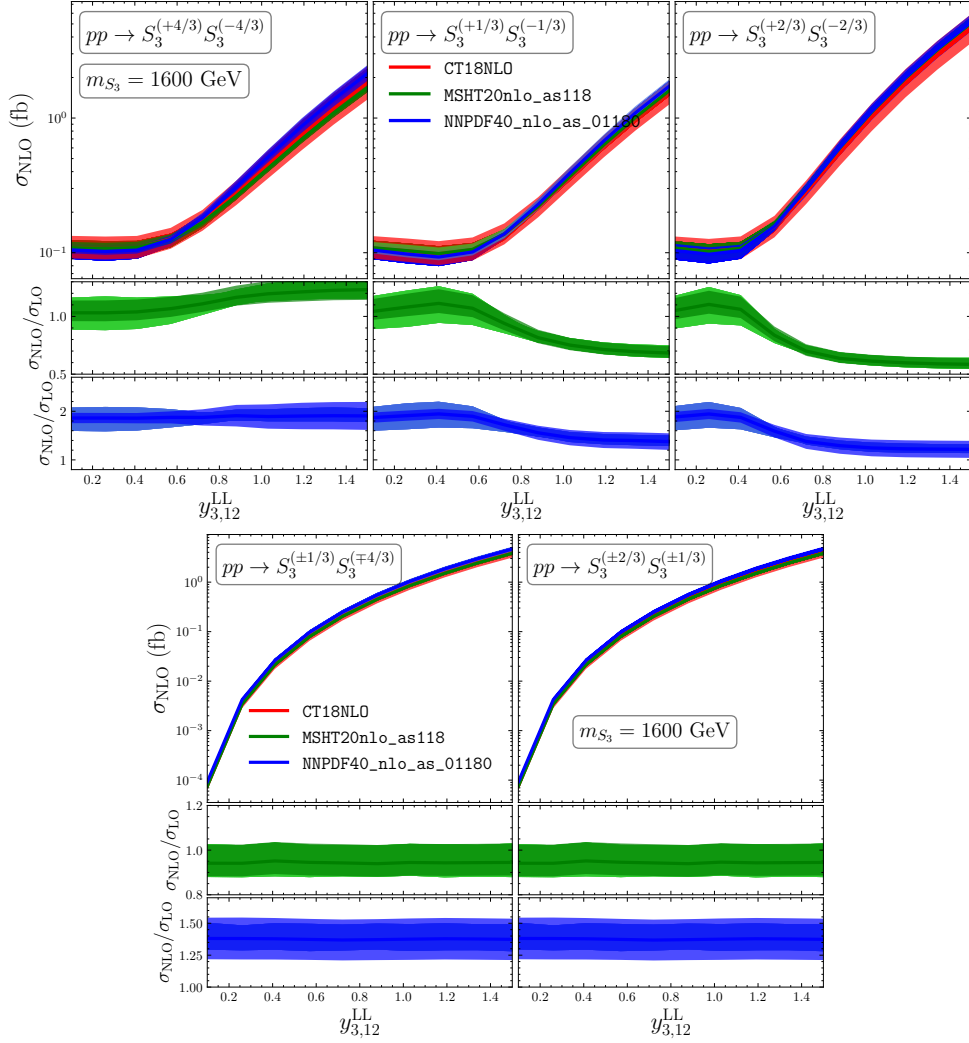


Figure 3. Same as in figure 2 but for processes involving solely S_3 leptoquark eigenstates. In the upper panels, we shown results as a function of $y = y_{3,12}^{LL}$ for the diagonal channels, *i.e.* $pp \rightarrow S_3^{(+4/3)} S_3^{(-4/3)}$ (left), $pp \rightarrow S_3^{(+1/3)} S_3^{(-1/3)}$ (middle) and $pp \rightarrow S_3^{(+2/3)} S_3^{(-2/3)}$ (right), whereas in the lower panels we focus on the off-diagonal production modes $pp \rightarrow S_3^{(\pm 1/3)} S_3^{(\mp 4/3)}$ (left) and $pp \rightarrow S_3^{(\pm 2/3)} S_3^{(\pm 1/3)}$ (right).

for all parton densities considered, both for the diagonal and the off-diagonal channels. As expected, there is no dependence of the NLO-QCD K -factor on the value of the Yukawa coupling in the off-diagonal case, as the y^4 dependence of the cross section cancels out in the ratio. Conversely, in the diagonal production modes the K factor dependence on y clearly depicts the transition (around $y \sim 0.6$) between the region of the parameter space in which the cross section is dominated by QCD diagrams, and that in which it is dominated by t -channel diagrams.

In figure 3 we consider the production of a pair of S_3 leptoquark eigenstates, the

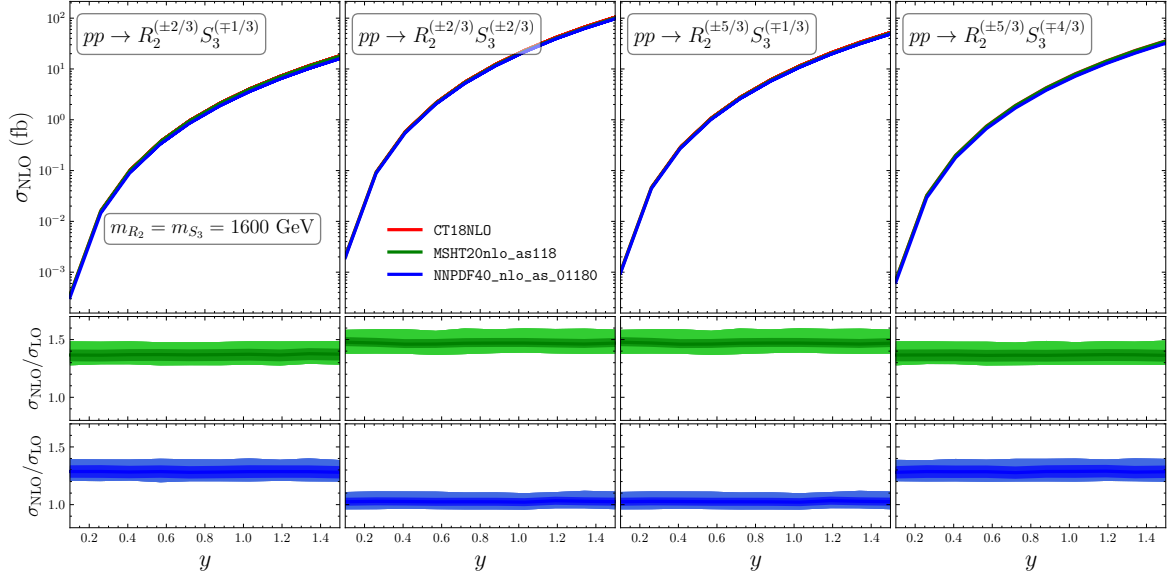


Figure 4. Same as in figure 2 but for the off-diagonal processes $pp \rightarrow R_2^{(\pm 2/3)} S_3^{(\mp 1/3)}$ (first column), $pp \rightarrow R_2^{(\pm 2/3)} S_3^{(\pm 2/3)}$ (second column), $pp \rightarrow R_2^{(\pm 5/3)} S_3^{(\mp 1/3)}$ (third column) and $pp \rightarrow R_2^{(\pm 5/3)} S_3^{(\mp 4/3)}$ (fourth column). Cross sections and K -factors are presented as a function of the leptoquark Yukawa coupling $y = y_{2,12}^{\text{LR}} = y_{3,12}^{\text{LL}}$.

leptoquark mass being fixed again to 1600 GeV. In the top row of the figure, we study the dependence of the cross sections and the K -factors on the Yukawa coupling $y = y_{3,12}^{\text{LL}}$ for the three diagonal processes ($pp \rightarrow S_3^{(+4/3)} S_3^{(-4/3)}$, $pp \rightarrow S_3^{(+1/3)} S_3^{(-1/3)}$ and $pp \rightarrow S_3^{(+2/3)} S_3^{(-2/3)}$), whereas the bottom row of the figure is dedicated to predictions for the off-diagonal production modes ($pp \rightarrow S_3^{(\pm 1/3)} S_3^{(\mp 4/3)}$ and $pp \rightarrow S_3^{(\pm 2/3)} S_3^{(\pm 1/3)}$). Cross sections for the production of a diagonal pair of S_3 leptoquark states feature characteristics that are very similar to those associated with the diagonal production of a pair of R_2 leptoquark eigenstates, which we studied in figure 2. NLO predictions indeed grow with increasing Yukawa coupling values due to t -channel contributions that are more and more important and that significantly impact rates once they become non-negligible relative to QCD contributions. In addition, NLO predictions obtained with the three PDF sets considered agree within their errors.

For the $pp \rightarrow S_3^{(+2/3)} S_3^{(-2/3)}$ and $pp \rightarrow S_3^{(+1/3)} S_3^{(-1/3)}$ processes, NLO K -factors are found to exhibit a similar behaviour as for the R_2 diagonal production modes, with a change of behaviour at $y \sim 0.4\text{--}0.6$ which corresponds to the threshold at which t -channel diagrams start to contribute. For the $pp \rightarrow S_3^{(+4/3)} S_3^{(-4/3)}$ process, the Yukawa coupling value at which t -channel diagrams start to contribute is similar ($y \sim 0.4\text{--}0.6$), but the K -factor value increases, instead of decreases. This different behaviour originates from the related t -channel contributions that are solely $d\bar{d}$ initiated, unlike for the other two diagonal processes for which up-type quarks contribute. For all three diagonal processes,

K -factors are found to affect LO cross sections by a few dozens of percent to up to a factor of 2, the exact value depending on the chosen PDF sets.

We now consider the off-diagonal processes $pp \rightarrow S_3^{(\pm 1/3)} S_3^{(\mp 4/3)}$ as well as $pp \rightarrow S_3^{(\pm 2/3)} S_3^{(\pm 1/3)}$, which we discuss together with processes in which one eigenstate from the R_2 multiplet is produced in association with one eigenstate from the S_3 multiplet, $pp \rightarrow R_2^{(\pm 2/3)} S_3^{(\mp 1/3)}$, $pp \rightarrow R_2^{(\pm 2/3)} S_3^{(\pm 2/3)}$, $pp \rightarrow R_2^{(\pm 5/3)} S_3^{(\mp 1/3)}$, and $pp \rightarrow R_2^{(\pm 5/3)} S_3^{(\mp 4/3)}$. Cross sections and K -factors are respectively shown in the bottom row of figure 3, and in figure 4. Qualitatively, they all present features that are very similar to those arising in $R_2^{(\pm 2/3)} R_2^{(\mp 5/3)}$ production. Cross section predictions at NLO are independent of the parton density choice (within uncertainties), and the K -factors are constant as the Yukawa coupling dependence in y^4 cancels out in the NLO to LO cross section ratios. We refer to appendix A for general details on the cross section dependence on the different Yukawa couplings entering the Lagrangian (2.1), that we take all equal here for simplicity. However, the obtained values for the K -factors associated with the various processes depend on the chosen PDF set, which is due to differences inherent to the MSHT2010_as_130 and NNPDF40_lo_as_01180 LO sets.

Crucially, at large values of the Yukawa coupling y , the NLO cross sections are substantially higher for processes involving leptoquarks of two different species than for any of the other processes considered here (both the diagonal channels and the production of a pair of different leptoquark eigenstates of the same species). The reason stems from the necessity of producing such a final state, that carries a total fermion number ($F = 3B + L$, with B and L being the baryon and lepton quantum numbers) equal to 2, from a pair of valence quarks [77].

3.3 t -channel and off-diagonal contributions on inclusive leptoquark production rates in the R_2 – S_3 model

In this section, we discuss the relevance of the off-diagonal leptoquark production modes with respect to the diagonal ones, for which we distinguish the pure QCD contributions from the ‘full’ total cross section including both QCD and t -channel diagrams. We begin our study with the second R_2 – S_3 scenario considered in section 2.2.1, in which all S_3 leptoquark eigenstates are decoupled. We correspondingly display results obtained in an ‘ R_2 -only’ model, as a function of a single non-zero Yukawa coupling that is taken to be either $y_{2,12}^{\text{LR}}$ or $y_{2,22}^{\text{LR}}$. We then investigate the impact of both leptoquark species in the first scenario introduced in section 2.2.1, for which we show predictions depending on $y_{2,12}^{\text{LR}} = y_{2,12}^{\text{RL}} = y_{3,12}^{\text{LL}}$.

In figure 5 we estimate the impact of the t -channel contributions on the various leptoquark pair production channels (upper panel of the figures). We consider LO (left) and NLO (right) total rates associated with the two diagonal channels as well as with the single

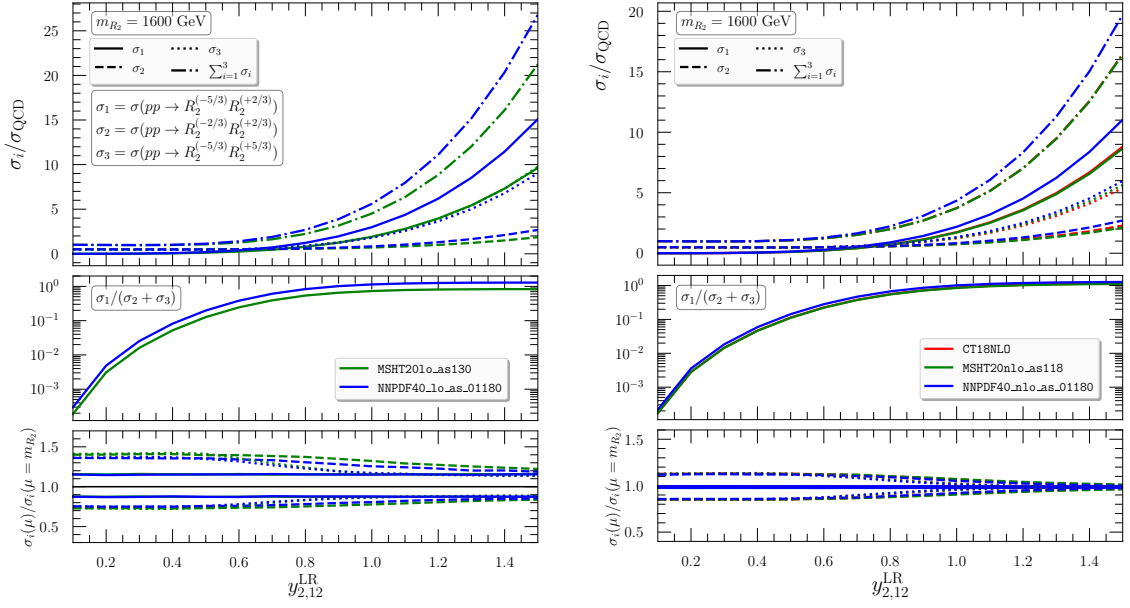


Figure 5. *Upper panels:* ratios of various R_2 leptoquark pair production cross sections of (3.1) to the QCD-driven cross section (3.2). Predictions are presented as a function of $y_{2,12}^{\text{LR}}$, for $m_{LQ} = 1600$ GeV, both at LO (left) and NLO (right). *Middle panels:* ratio of the off-diagonal leptoquark pair production cross section σ_1 to the total diagonal pair production cross section $\sigma_2 + \sigma_3$. *Lower panels:* dependence of σ_i (for $i = 1, 2, 3$) on the renormalisation and factorisation scales when they are varied simultaneously by a factor of 2 up and down.

off-diagonal channel relevant for a model in which only an R_2 leptoquark is included,

$$\begin{aligned}
 \sigma_1 &\equiv \sigma \left[pp \rightarrow R_2^{(\pm 5/3)} R_2^{(\mp 2/3)} \right], \\
 \sigma_2 &\equiv \sigma \left[pp \rightarrow R_2^{(-2/3)} R_2^{(+2/3)} \right], \\
 \sigma_3 &\equiv \sigma \left[pp \rightarrow R_2^{(-5/3)} R_2^{(+5/3)} \right].
 \end{aligned} \tag{3.1}$$

The results are presented in the form of ratios to the cross section σ_{QCD} associated with the QCD-driven production of identical R_2 states,

$$\sigma_{\text{QCD}} \equiv \sigma \left[pp \rightarrow R_2^{(-5/3)} R_2^{(+5/3)} \right] + \sigma \left[pp \rightarrow R_2^{(-2/3)} R_2^{(+2/3)} \right] \quad \text{for } y_{2,12}^{\text{LR}} = 0, \tag{3.2}$$

and we study the dependence of these ratios on the Yukawa coupling $y_{2,12}^{\text{LR}}$ (all other Yukawa couplings being set to zero). In the middle panel of the figures, we investigate the importance of the off-diagonal cross section σ_1 relative to the sum of the diagonal ones $\sigma_2 + \sigma_3$ (with t -channel contributions included), whereas the lower panel of the figures is dedicated to the scale uncertainties inherent to each of the three processes. Moreover, all results are shown for all PDF choices considered.

When $y_{2,12}^{\text{LR}}$ is small, the ratios $\sigma_{2,3}/\sigma_{\text{QCD}}$ are close to 0.5 for each of the diagonal modes, while $\sigma_1/\sigma_{\text{QCD}}$ is close to 0 in the off-diagonal case. The t -channel effects are

indeed small and negligible relative to the QCD rates, that only depend on the leptoquark mass. For larger $y_{2,12}^{\text{LR}}$ values, t -channel contributions kick in and quickly dominate with increasing Yukawa couplings. Cross sections corresponding to the diagonal production rates become much larger than in the pure QCD case, and the off-diagonal mode even gets larger than the diagonal channels. In other words, the rise of the cross section due to t -channel contributions in a specific diagonal production mode is smaller than the rise of the cross section of the off-diagonal mode, whilst both these rises are significant. In addition, the middle panel of the figure indicates that the off-diagonal cross section is mostly equal to the sum of the cross sections of the two diagonal modes (including t -channel contributions) for large $y_{2,12}^{\text{LR}}$ values.

Comparing NLO (right panel) with LO (left panel) predictions, it turns out that LO-based analyses are not reliable to judge the importance of both the off-diagonal and the diagonal modes with respect to the pure QCD case (when the Yukawa couplings are moderate or large). NLO corrections are indeed very relevant for all modes, and they affect differently QCD-driven and t -channel-driven diagrams. The $\sigma_1/(\sigma_2 + \sigma_3)$ ratio stays however relatively insensitive to the precision of the perturbative calculation (middle panel of the figures). In addition, this ratio is quite robust relative to the chosen set of PDFs, and this is even more true at NLO. On the other hand, the ratios in the upper panels of the plots significantly disagree with each other when the employed PDF set is varied.

In the lower panels of the figures, we show the relative size of the theoretical errors originating from scale variation for each of the three production modes, and for the different PDF set considered. Receiving a significant contribution from pure QCD diagrams, the diagonal modes are in principle plagued with a bigger theoretical error than the off-diagonal one. However, at large values of $y_{2,12}^{\text{LR}}$, *i.e.* when the importance of the pure QCD contributions diminishes, the size of the theoretical error gradually becomes independent of the production channel. Finally, as expected the size of scale variation errors gets significantly smaller at NLO (by at least a factor of 3), and is mostly independent of the chosen PDF set.

In figure 6, we display the results of a similar study, but for an R_2 leptoquark scenario in which $y_{2,22}^{\text{LR}}$ is left free to be varied and all other Yukawa couplings are fixed to zero. The difference in the behaviour of the various cross sections from eq. (3.1) relative to the results shown in figure 5 is quite dramatic, and it is mostly due to the different possibilities for the initial states. At tree-level and when solely the Yukawa coupling $y_{2,22}^{\text{LR}}$ is non-zero, there is no option for a t -channel subprocess involving an initial valence quark to contribute. This reduces the potential impact of all (diagonal and off-diagonal) t -channel contributions, as visible from the upper panels of the figure. The ratios of the three leptoquark production rates to the pure QCD result (3.2) are indeed much lower at large values of the Yukawa coupling than in figure 5. In addition, the diagonal production modes dominate, with

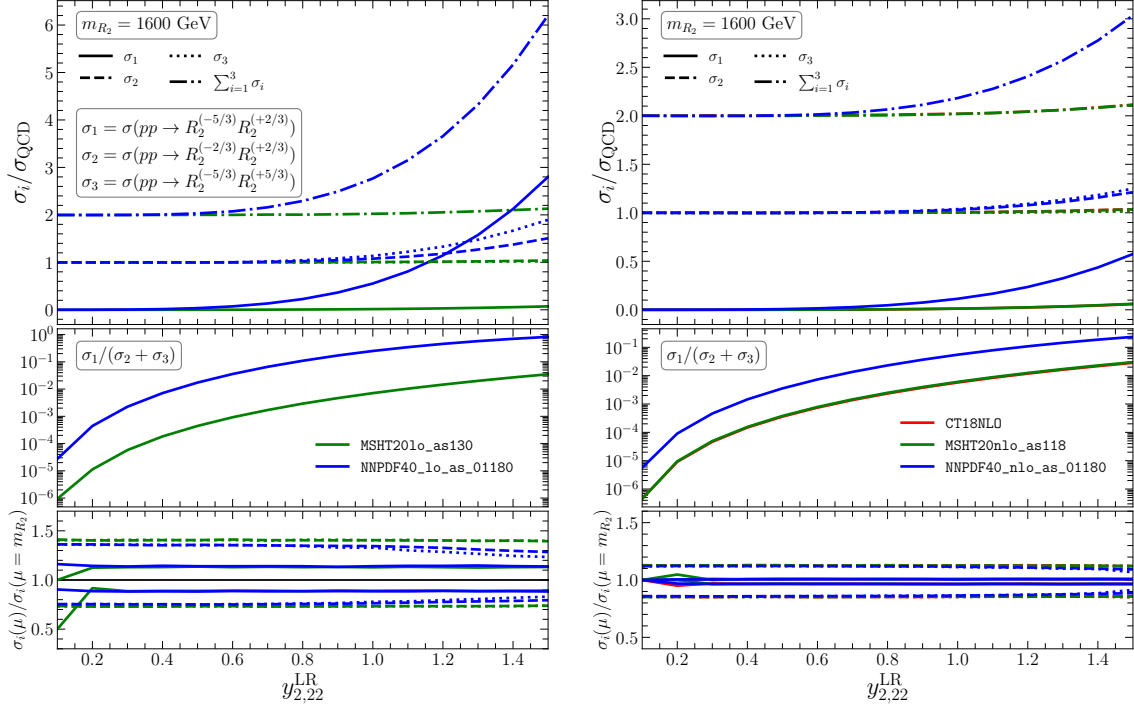


Figure 6. Same as in figure 5 but for an R_2 leptoquarks scenario in which the only non-zero Yukawa coupling is $y_{2,22}^{\text{LR}}$.

cross sections that are a few times larger than that of the off-diagonal mode (see the middle panels of the figure). Accordingly, theoretical uncertainties due to scale variation are almost independent of $y_{2,22}^{\text{LR}}$ for the diagonal channels, and larger in these cases than in the off-diagonal case.

Our results also depict a much higher dependence on the PDF set used in the calculations. Predictions obtained with NNPDF4.0 densities are indeed much different from those obtained with either CT18 or MSHT20 PDFs (that agree with each other at NLO). For instance, the ratio $\sigma_1/(\sigma_2 + \sigma_3)$ differs at NLO by as much as one order of magnitude when comparing MSHT20 and NNPDF4.0 predictions. We attribute these large difference to the treatment of the charm quark distribution in the PDF fitting procedure, that is independently parametrised in the default NNPDF4.0 case and fully perturbatively treated in the CT18 and MSHT20 cases (see also section 4).

After studying the relevance of the off-diagonal modes in the simpler R_2 model with only one non-zero Yukawa coupling, we consider cross sections in the R_2 - S_3 model in figure 7. In the top four panels of the figure we present ratios of the production cross sections associated with a specific process to the sum all pure QCD contributions, at LO

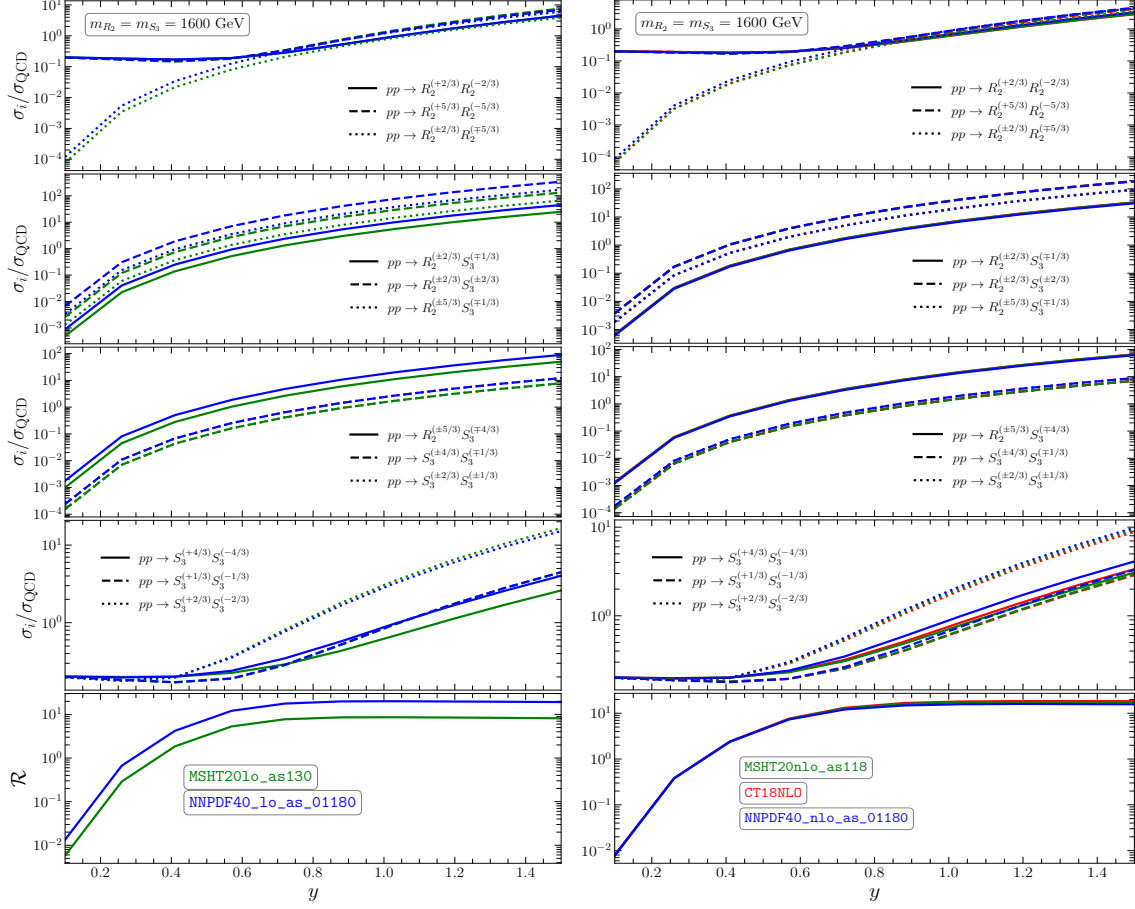


Figure 7. Upper four panels: ratios of the different scalar leptoquark pair production cross section with respect to the pure QCD contribution as a function of $y = y_{2,12}^{\text{LR}} = y_{2,12}^{\text{RL}} = y_{3,12}^{\text{LL}}$ at LO (left) and NLO (right). σ_{QCD} is defined as the sum of the cross sections for all diagonal channels with $y = 0$, all predictions correspond to $m_{R_2} = m_{S_3} = 1600$ GeV. Lower panel: ratio (3.4) of the (full) off-diagonal production rate to (full) the diagonal one as a function of y .

(left figure) and NLO (right figure). Here,

$$\begin{aligned} \sigma_{\text{QCD}} \equiv & \sigma[pp \rightarrow R_2^{(-5/3)} R_2^{(+5/3)}] + \sigma[pp \rightarrow R_2^{(-2/3)} R_2^{(+2/3)}] + \sigma[pp \rightarrow S_3^{(-4/3)} S_3^{(+4/3)}] \\ & + \sigma[pp \rightarrow S_3^{(-2/3)} S_3^{(+2/3)}] + \sigma[pp \rightarrow S_3^{(-1/3)} S_3^{(+1/3)}] \quad \text{for } y = 0. \end{aligned} \quad (3.3)$$

NLO corrections can lead to a significant change of the ratios, often by tens of percent or more. Furthermore, at high enough values of the Yukawa coupling off-diagonal channels and t -channel diagonal contributions dominate over pure QCD production. This dominance reaches factors of 10–100, and is most pronounced for off-diagonal processes involving two valence quarks.

The relative importance of the off-diagonal modes can be also judged by considering the ratio of the cross section for all possible off-diagonal production modes allowed in the

model to that of all diagonal production modes (including t -channel contributions). This ratio is defined by

$$\mathcal{R} = \frac{\sum_{i \neq j} \sigma [pp \rightarrow \text{LQ}_i \text{LQ}_j]}{\sum_i \sigma [pp \rightarrow \text{LQ}_i \text{LQ}_i]}. \quad (3.4)$$

and is shown in the lowest panel in figure 7. In the particular model considered here, the off-diagonal-channels become as important as the diagonal ones at an already relative small values of $y \sim 0.35$. Furthermore, at $y \gtrsim 1$ off-diagonal leptoquark pair production is around 20 times higher than diagonal leptoquark pair production. Comparing with the previously studied R_2 model, we observe that this behaviour is entirely driven by the possibility to produce a pair of leptoquarks from an initial state including one or more valence quarks. Whereas in the R_2 model the off-diagonal $R_2^{(\pm 2/3)} R_2^{(\mp 5/3)}$ production involves at LO a $d\bar{u}/\bar{d}u$ initial state, $R_2^{(\pm 2/3)} S_3^{(\pm 2/3)}$ production originates from $uu/\bar{u}\bar{u}$ scattering.

Results for the same scenarios as discussed in this section, but with a higher leptoquark mass of $m_{\text{LQ}} = 2400$ GeV, are presented in appendix B.

4 Role of the off-diagonal production modes in scenarios addressing the flavour anomalies

In this section, we discuss predictions for scalar leptoquark production processes in the context of the benchmark scenarios introduced in section 2.2.2, and we evaluate the impact of the off-diagonal production channels relatively to the diagonal ones. Whereas the latter have been already studied in [60], we provide predictions for completeness. Moreover, in the case of results obtained with the NNPDF set, we update our predictions by making use of the latest version 4.0 of their fit.

4.1 Total cross sections at NLO

In tables 4, 5, and 6, we show predictions for NLO-QCD total cross sections of all leptoquark pair production modes relevant for the R_2 , R_2 - S_3 , and S_1 - S_3 scenarios of section 2.2.2, respectively. Our results include scale and PDF uncertainties, and we only consider processes for which the cross section is larger than 1 ab for at least one of the three PDF sets used.

Off-diagonal contributions are generally small for all selected benchmark points. For scenarios a_1 and a_2 in the R_2 model, they are indeed negligible, with rates falling below 1 ab. They are thus not shown in table 4. For benchmarks b_1 and b_2 in the R_2 - S_3 model, there exist two off-diagonal channels with cross sections larger than 1 ab, $pp \rightarrow R_2^{(\pm 5/3)} S_3^{(\mp 4/3)}$ and $pp \rightarrow R_2^{(\pm 2/3)} S_3^{(\mp 1/3)}$, for which the rates are therefore reported in table 5. They consist of about 0.1% to 2% of the *full* leptoquark pair-production cross section (where all channels are summed over), the precise number depending on the benchmark point and on

		CT18NLO	MSHT20_nlo_as_0118	NNPDF40_nlo_as_01180
a_1	$R_2^{(+2/3)} R_2^{(-2/3)}$	$6.89^{+7.7\%+18.8\%}_{-9.6\%-13.7\%}$	$6.82^{+7.2\%+8.2\%}_{-10.6\%-5.7\%}$	$11.17^{+3.0\%+25.2\%}_{-4.2\%-25.2\%}$
	$R_2^{(+5/3)} R_2^{(-5/3)}$	$6.87^{+8.3\%+18.9\%}_{-9.8\%-13.7\%}$	$6.86^{+7.9\%+8.2\%}_{-10.2\%-5.7\%}$	$11.15^{+3.5\%+25.2\%}_{-4.0\%-25.2\%}$
a_2	$R_2^{(+2/3)} R_2^{(-2/3)}$	$5.49^{+12.2\%+13.8\%}_{-13.0\%-10.4\%}$	$5.56^{+13.2\%+5.9\%}_{-11.7\%-4.1\%}$	$5.37^{+10.7\%+2.7\%}_{-12.4\%-2.7\%}$
	$R_2^{(+5/3)} R_2^{(-5/3)}$	$5.48^{+11.2\%+13.8\%}_{-13.1\%-10.4\%}$	$5.57^{+13.5\%+5.9\%}_{-11.7\%-4.1\%}$	$5.37^{+10.4\%+2.7\%}_{-12.9\%-2.7\%}$

Table 4. Total cross sections at NLO-QCD (in fb) for the a_1 and a_2 benchmark points of table 1. Our predictions include t -channel contributions, scale uncertainties (first errors reported) and PDF uncertainties (second errors reported). Cross sections below 1 ab are not shown.

		CT18NLO	MSHT20_nlo_as_0118	NNPDF40_nlo_as_01180
b_1	$R_2^{(+2/3)} R_2^{(-2/3)}$	$0.708^{+11.3\%+18.1\%}_{-14.3\%-13.4\%}$	$0.712^{+12.7\%+7.9\%}_{-12.9\%-5.4\%}$	$0.714^{+10.0\%+4.9\%}_{-12.2\%-4.9\%}$
	$R_2^{(+5/3)} R_2^{(-5/3)}$	$0.706^{+11.1\%+18.1\%}_{-13.9\%-13.4\%}$	$0.712^{+13.3\%+7.9\%}_{-13.3\%-5.4\%}$	$0.715^{+9.5\%+4.8\%}_{-12.8\%-4.8\%}$
	$S_3^{(+2/3)} S_3^{(-2/3)}$	$0.0107^{+15.4\%+30.5\%}_{-14.9\%-21.7\%}$	$0.0109^{+15.9\%+14.5\%}_{-14.3\%-9.8\%}$	$0.0110^{+12.3\%+9.1\%}_{-14.7\%-9.1\%}$
	$S_3^{(+1/3)} S_3^{(-1/3)}$	$0.0108^{+14.6\%+30.5\%}_{-15.7\%-21.7\%}$	$0.0110^{+15.7\%+14.5\%}_{-14.5\%-9.8\%}$	$0.0111^{+12.0\%+9.1\%}_{-14.9\%-9.1\%}$
	$S_3^{(+4/3)} S_3^{(-4/3)}$	$0.0108^{+14.2\%+30.7\%}_{-16.0\%-21.8\%}$	$0.0110^{+15.2\%+14.7\%}_{-14.8\%-9.9\%}$	$0.0111^{+11.6\%+9.1\%}_{-14.5\%-9.1\%}$
	$R_2^{(\pm 5/3)} S_3^{(\mp 4/3)}$	$0.0014^{+5.0\%+72.1\%}_{-5.2\%-46.2\%}$	$0.00144^{+8.9\%+32.2\%}_{-2.2\%-21.3\%}$	$0.0066^{+4.4\%+44.3\%}_{-5.5\%-44.3\%}$
	$R_2^{(\pm 2/3)} S_3^{(\mp 1/3)}$	$0.00069^{+5.0\%+72.1\%}_{-5.2\%-46.1\%}$	$0.00072^{+8.6\%+32.1\%}_{-2.5\%-21.2\%}$	$0.0033^{+4.7\%+44.2\%}_{-5.3\%-44.2\%}$
b_2	$R_2^{(+2/3)} R_2^{(-2/3)}$	$0.719^{+11.8\%+18.9\%}_{-13.4\%-13.9\%}$	$0.726^{+13.2\%+8.3\%}_{-12.1\%-5.7\%}$	$0.832^{+8.1\%+11.9\%}_{-10.8\%-11.9\%}$
	$R_2^{(+5/3)} R_2^{(-5/3)}$	$0.719^{+11.5\%+18.8\%}_{-13.3\%-13.8\%}$	$0.727^{+12.9\%+8.2\%}_{-12.6\%-5.6\%}$	$0.834^{+7.5\%+11.9\%}_{-10.8\% \ 11.9\%}$
	$S_3^{(+2/3)} S_3^{(-2/3)}$	$0.0107^{+15.4\%+30.5\%}_{-15.0\%-21.7\%}$	$0.0109^{+15.9\%+14.5\%}_{-14.3\%-9.8\%}$	$0.0110^{+12.7\%+9.1\%}_{-14.7\%-9.1\%}$
	$S_3^{(+1/3)} S_3^{(-1/3)}$	$0.0108^{+14.3\%+30.7\%}_{-15.8\%-21.8\%}$	$0.0110^{+15.6\%+14.6\%}_{-14.3\%-9.9\%}$	$0.0108^{+11.5\%+9.1\%}_{-14.7\%-9.1\%}$
	$S_3^{(+4/3)} S_3^{(-4/3)}$	$0.0109^{+14.0\%+31.5\%}_{-15.1\%-22.2\%}$	$0.0111^{+15.6\%+15.1\%}_{-14.1\%-10.2\%}$	$0.0115^{+11.8\%+9.1\%}_{-14.2\%-9.1\%}$
	$R_2^{(\pm 5/3)} S_3^{(\mp 4/3)}$	$0.0048^{+4.9\%+72.2\%}_{-5.4\%-46.2\%}$	$0.0049^{+9.3\%+32.1\%}_{-2.4\%-21.3\%}$	$0.0227^{+4.4\%+44.2\%}_{-5.6\%-44.2\%}$
	$R_2^{(\pm 2/3)} S_3^{(\mp 1/3)}$	$0.0024^{+4.9\%+72.1\%}_{-5.2\%-46.1\%}$	$0.0025^{+8.4\%+32.1\%}_{-2.5\%-21.3\%}$	$0.0113^{+4.6\%+44.2\%}_{-5.3\%-44.2\%}$

Table 5. Same as table 4 but for the b_1 and b_2 scenarios of table 2.

the employed PDF set. The scaling relation between the two off-diagonal channels is not surprising, and could be actually expected from eq. (A.10). For benchmarks c_1 and c_2 in the S_1 – S_3 model, four channels are associated with rates larger than 1 ab, and are thus displayed in table 6: $pp \rightarrow S_1^{(\pm 1/3)} S_3^{(\mp 1/3)}$, $pp \rightarrow S_1^{(\pm 1/3)} S_3^{(\pm 2/3)}$, $pp \rightarrow S_3^{(\pm 2/3)} S_3^{(\pm 1/3)}$, and $pp \rightarrow S_3^{(\pm 1/3)} S_3^{(\mp 4/3)}$. When CT18 and MSHT20 parton densities are used, they impact the *full* leptoquark pair production rate by 1% to 8%, depending on the scenario, and

		CT18NLO	MSHT20_nlo_as_0118	NNPDF40_nlo_as_01180
c_1	$S_1^{(+1/3)} S_1^{(-1/3)}$	$1.45^{+10.4\%+18.7\%}_{-12.8\%-13.0\%}$	$1.47^{+12.3\%+7.8\%}_{-10.9\%-5.4\%}$	$1.78^{+6.6\%+10.8\%}_{-8.9\%-10.8\%}$
	$S_3^{(+2/3)} S_3^{(-2/3)}$	$1.35^{+11.3\%+16.3\%}_{-14.3\%-12.2\%}$	$1.36^{+12.9\%+7.1\%}_{-12.8\%-4.9\%}$	$1.30^{+10.9\%+3.5\%}_{-13.2\%-3.5\%}$
	$S_3^{(+1/3)} S_3^{(-1/3)}$	$1.35^{+11.9\%+16.3\%}_{-13.9\%-12.2\%}$	$1.36^{+13.4\%+7.1\%}_{-13.0\%-4.9\%}$	$1.29^{+10.7\%+3.5\%}_{-14.3\%-3.5\%}$
	$S_3^{(+4/3)} S_3^{(-4/3)}$	$1.35^{+11.9\%+16.4\%}_{-13.6\%-12.2\%}$	$1.37^{+12.6\%+7.1\%}_{-12.8\%-4.9\%}$	$1.30^{+10.8\%+3.5\%}_{-13.1\%-3.5\%}$
	$S_1^{(\pm 1/3)} S_3^{(\mp 1/3)}$	$0.036^{+4.3\%+115.0\%}_{-5.4\%-33.1\%}$	$0.038^{+10.2\%+24.5\%}_{-0.1\%-19.6\%}$	$0.14^{+4.1\%+35.7\%}_{-5.8\%-35.7\%}$
	$S_1^{(\pm 1/3)} S_3^{(\pm 2/3)}$	$0.032^{+4.4\%+71.7\%}_{-5.2\%-30.8\%}$	$0.034^{+9.9\%+22.7\%}_{-0.2\%-15.8\%}$	$0.15^{+4.6\%+38.2\%}_{-5.2\%-38.2\%}$
	$S_3^{(\pm 2/3)} S_3^{(\pm 1/3)}$	$0.0051^{+4.9\%+71.3\%}_{-4.4\%-30.8\%}$	$0.0054^{+10.7\%+22.7\%}_{-0.1\%-15.8\%}$	$0.0239^{+4.3\%+38.2\%}_{-5.7\%-38.2\%}$
	$S_3^{(\pm 1/3)} S_3^{(\mp 4/3)}$	$0.0051^{+4.9\%+71.1\%}_{-4.4\%-30.8\%}$	$0.0054^{+10.8\%+22.8\%}_{-0.2\%-15.7\%}$	$0.0239^{+4.5\%+38.1\%}_{-5.8\%-38.1\%}$
c_2	$S_1^{(+1/3)} S_1^{(-1/3)}$	$1.44^{+10.4\%+18.2\%}_{-12.9\%-13.0\%}$	$1.46^{+12.0\%+7.7\%}_{-11.8\%-5.3\%}$	$1.73^{+7.2\%+10.8\%}_{-9.1\%-10.8\%}$
	$S_3^{(+2/3)} S_3^{(-2/3)}$	$1.41^{+10.6\%+17.5\%}_{-13.4\%-13.0\%}$	$1.41^{+12.1\%+7.6\%}_{-12.1\%-5.3\%}$	$1.64^{+6.9\%+12.1\%}_{-10.1\%-12.1\%}$
	$S_3^{(+1/3)} S_3^{(-1/3)}$	$1.39^{+11.1\%+17.0\%}_{-13.3\%-12.5\%}$	$1.40^{+12.9\%+7.3\%}_{-11.9\%-5.0\%}$	$1.47^{+9.4\%+5.1\%}_{-11.9\%-5.1\%}$
	$S_3^{(+4/3)} S_3^{(-4/3)}$	$1.48^{+10.9\%+22.1\%}_{-12.2\%-13.0\%}$	$1.52^{+13.0\%+7.9\%}_{-9.7\%-5.5\%}$	$1.74^{+7.2\%+10.0\%}_{-9.4\%-10.0\%}$
	$S_1^{(\pm 1/3)} S_3^{(\mp 1/3)}$	$0.138^{+4.7\%+115.0\%}_{-5.1\%-33.1\%}$	$0.146^{+9.7\%+24.6\%}_{-0.2\%-19.7\%}$	$0.553^{+4.1\%+35.8\%}_{-5.8\%-35.8\%}$
	$S_1^{(\pm 1/3)} S_3^{(\pm 2/3)}$	$0.125^{+4.4\%+71.6\%}_{-6.7\%-30.9\%}$	$0.132^{+9.8\%+22.7\%}_{-0.1\%-15.8\%}$	$0.588^{+4.6\%+38.2\%}_{-5.3\%-38.2\%}$
	$S_3^{(\pm 2/3)} S_3^{(\pm 1/3)}$	$0.102^{+5.0\%+71.9\%}_{-4.8\%-30.8\%}$	$0.108^{+11.0\%+23.0\%}_{-0.2\%-15.8\%}$	$0.481^{+4.3\%+38.1\%}_{-5.7\%-38.1\%}$
	$S_3^{(\pm 1/3)} S_3^{(\mp 4/3)}$	$0.102^{+5.1\%+71.7\%}_{-4.2\%-30.9\%}$	$0.108^{+10.9\%+22.8\%}_{-0.5\%-15.8\%}$	$0.481^{+4.5\%+38.1\%}_{-5.8\%-38.1\%}$

Table 6. Same as table 4 but for the c_1 and c_2 scenarios of table 3.

those values increase to 5% and 25% when the NNPDF4.0 set is employed. This large difference in the predictions can be attributed to the different treatment of the charm distribution in the NNPDF set, as discussed more extensively in section 4.2. Moreover, the relative impact of the off-diagonal contributions is directly connected to the strength of the leptoquark coupling to second-generation quarks with respect to all other Yukawa couplings. Consequently, off-diagonal channels play a bigger role in scenarios b_2 and c_2 relatively to scenarios b_1 and c_1 , due to the larger values of the couplings $y_{2,23}^{\text{RL}}$ (in b_2) and $y_{3,23}^{\text{LL}}$ (in c_2), respectively.

NLO corrections are also known to generally reduce scale uncertainties. In this context, it can be seen that for all off-diagonal channels, scale uncertainties get smaller than these inherent to the diagonal channels. This originates from the absence of $\mathcal{O}(\alpha_s^2)$ contributions at LO in the off-diagonal case. On the contrary, PDF uncertainties in the off-diagonal

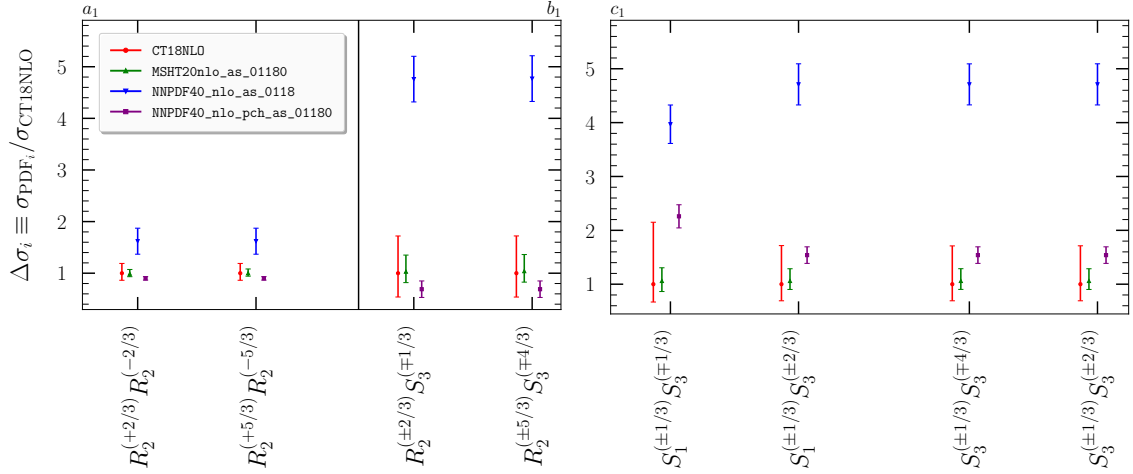


Figure 8. Total cross section predictions, with the associated PDF uncertainties, for a selection of processes in scenario a_1 (left panel of left figure; see also table 4), b_1 (right panel of left figure; see also table 5), and c_1 (right figure; see also table 6). Predictions are normalised to the cross section obtained with the central CT18NLO PDF set.

channels are significantly increased by a factor of at least 2, due to the strong dependence of the rates on the heavy sea-quark distributions.

Our results therefore show that once NLO-QCD predictions are considered, off-diagonal leptoquark pair-production channels generally lead to an irrelevant contribution to the *full* leptoquark pair production rate for scenarios motivated by the flavour anomalies. Exceptions however exist, as shown with the benchmarks c_1 and c_2 , where effects reaching tens of percent are observed.

4.2 Impact of the charm PDF on the predictions

Due to the inclusion of t -channel and off-diagonal contributions, leptoquark pair production becomes more strongly dependent on the specific quark flavours triggered by the structure of the associated Yukawa couplings. Consequently, the way the charm density is accounted for in parton density fits may impact predictions for scenarios where leptoquarks interact with second-generation quarks. This is in particular relevant to understand the large differences observed between predictions obtained with the CT18/MSHT20 sets and those obtained with the NNPDF4.0 set. In order to further explore this feature, it must be noted that the NNPDF collaboration independently modeled an intrinsic charm contribution in their NNPDF4.0 baseline fit, and that it has alternatively released a set where the charm density purely arises perturbatively [92]. In the present section, we discuss the effect of these different NNPDF parametrisations of the charm quark distribution on the production rates, together with the associated uncertainties.

In figure 8, we display cross section predictions for a selection of processes from ta-

bles 4–6, for various PDF sets, and after including the corresponding PDF uncertainties. All results are normalised to predictions obtained with the central CT18NLO set. In addition to the three PDF sets considered so far, we additionally evaluate the different production cross sections with the NNPDF4.0 set involving a perturbative treatment of the charm (NNPDF4.0_nlo_pch_as_01180). Our results show that predictions obtained with the CT18, MSHT20 and NNPDF4.0 with perturbative charm sets all agree within their uncertainties, except for tensions arising in results for scenario c_1 . In contrast, NNPDF4.0 predictions with intrinsic charm are significantly larger than those obtained with any of the other sets of parton densities, the difference reaching a factor of 4–5 in the most extreme cases. The choice made for the charm parametrisation in the PDF fit has hence a large impact on our predictions.

5 Conclusions

In this work, we have studied diagonal and off-diagonal production modes of scalar leptoquark pairs at the LHC, taking into account NLO-QCD corrections and Yukawa-induced t -channel contributions. In particular, we have focused on generic simplified models involving either R_2 and S_3 leptoquarks or R_2 leptoquarks alone, as well as specific benchmark scenarios in R_2 , R_2 – S_3 , and S_1 – S_3 models addressing the flavour anomalies.

We find that in the cases studied here LO predictions are not reliable on their own. In order to obtain reliable theoretical predictions NLO corrections must be included. First, NLO corrections and the corresponding K -factors can be very big, both for diagonal and off-diagonal production. Their exact size depends of course on the specific process and the value of the Yukawa coupling, but they can reach from tens of percent up to a factor of 2 for $m_{LQ} = 1600$ GeV and a factor of about 4 for $m_{LQ} = 2400$ GeV. Secondly, LO predictions show a very strong dependence on the PDF sets used for the calculation. Adding NLO corrections dramatically improves the agreement between predictions obtained with different PDF sets. Furthermore, NLO corrections lead to reduced theoretical uncertainties both through the reduction of the scale dependence and the PDF error.

As can be expected, production rates for diagonal and off-diagonal modes grow with the value of the Yukawa coupling. While off-diagonal production is purely Yukawa coupling-induced (and therefore negligible at small values of the Yukawa coupling), diagonal leptoquark pair production involves t -channel contributions in addition to the pure QCD diagrams. The relevance of off-diagonal with respect to diagonal production including t -channel diagrams depends on the model, the process and the involved couplings. If a given off-diagonal process can proceed via two valence quarks in the initial state, it dominates at large values of the Yukawa coupling, with production rates much higher than for diagonal production (even with t -channel diagrams included). However, if there is no such PDF enhancement possible, at large values of the Yukawa coupling the rates for the off-diagonal

production are comparable or even smaller than those in the diagonal case. This clearly shows that in generic leptoquark models where large Yukawa couplings are relevant, in order to obtain reliable estimates of the pair-production rates at the LHC, one needs to consider – with NLO precision – not only the pure QCD cross sections but also the diagonal and off-diagonal t -channel contributions. Consequently, we urge both experimental and theoretical groups to use NLO predictions where these contributions are included instead of the LO ones.

We have also studied the relevance of the off-diagonal channels in a few scenarios addressing the flavour anomalies. We have found that for the benchmark points considered the off-diagonal production rates are in general small compared to the diagonal production. Again, the exact values depend on the model and the benchmark point but the effect ranges from negligible to $\mathcal{O}(10\%)$ of the total rate. In scenarios where leptoquarks couple to charm quarks, we observe that the different treatments applied to the charm quark distribution (perturbative or intrinsic) have a large impact on the theoretical predictions at NLO through the t -channel contributions, affecting in particular off-diagonal production.

Acknowledgements

The work of AJ is supported in part by a KIAS Individual Grant No. QP084401 via the Quantum Universe Center at Korea Institute for Advanced Study. The work of BF has been partly supported by the French Agence Nationale de la Recherche (ANR) under grant ANR-21-CE31-0013 (project DMwithLLPatLHC). AK acknowledges the support and hospitality of the CERN Theoretical Physics Department. The results of this study were obtained using the High Performance Computing facilities at the Center for Advanced Computation at KIAS.

A Leading-order amplitudes for off-diagonal leptoquark pair production

In this section, we consider the R_2 – S_3 simplified model introduced in section 2.2.1, and we investigate the dependence of the various leptoquark off-diagonal pair production channels on the model’s Yukawa couplings. We remind that all the entries of the coupling matrices are fixed to zero, except $y_{3,12}^{\text{LL}}$, $y_{2,12}^{\text{LR}}$, and $y_{2,12}^{\text{RL}}$. Moreover, we have imposed that all five leptoquark eigenstates are mass-degenerate, *i.e.* $m_{R_2} = m_{S_3} \equiv m_{\text{LQ}}$.

We consider generic off-diagonal leptoquark pair production processes,

$$a(k_1, c_1) \ b(k_2, c_2) \quad \rightarrow \quad \text{LQ}_i(k_3, c_3) \ \text{LQ}_j(k_4, c_4), \quad (\text{A.1})$$

where a, b are the initial annihilating partons, k_m with $m = 1, 2, 3, 4$ stand for the four-momenta of the different involved particles and c_m are the corresponding colour indices. Moreover, in our notation, the generic leptoquark indices i and j only refer to the fact that

the final-state leptoquarks are different. The R_2 - S_3 model contains various off-diagonal channels that can be categorised into three categories according to the total electric charge of the final state.

Charge $\pm 4/3$ – There are two partonic possibilities in the R_2 - S_3 model to produce a pair of leptoquarks whose total electric charge is equal to $+4/3$,

$$uu \rightarrow R_2^{(+2/3)} S_3^{(+2/3)} \quad \text{and} \quad uu \rightarrow R_2^{(+5/3)} S_3^{(-1/3)}. \quad (\text{A.2})$$

These modes proceed through the annihilation of two up-type quarks via the t -channel exchange of either a charged lepton or a neutrino. The corresponding amplitudes are given by

$$\begin{aligned} \mathcal{M}_{R_2^{(+2/3)} S_3^{(+2/3)}} &= -\sqrt{2} y_{2,12}^{\text{RL}} y_{3,12}^{\text{LL}} \left[(\bar{v}_1 P_L \not{k}_3 u_2) \frac{1}{\hat{u}} \delta_{c_1 c_4} \delta_{c_2 c_3} - (\bar{v}_1 P_R \not{k}_3 u_2) \frac{1}{\hat{t}} \delta_{c_1 c_3} \delta_{c_2 c_4} \right], \\ \mathcal{M}_{R_2^{(+5/3)} S_3^{(-1/3)}} &= y_{2,12}^{\text{LR}} y_{3,12}^{\text{LL}} \left[m_\mu \frac{1}{\hat{u}} (\bar{v}_1 P_L u_2) \delta_{c_1 c_4} \delta_{c_2 c_3} - (\bar{v}_1 P_L \not{k}_3 u_2) \frac{1}{\hat{u}} \delta_{c_1 c_4} \delta_{c_2 c_3} \right. \\ &\quad \left. + m_\mu (\bar{v}_1 P_L u_2) \frac{1}{\hat{t}} \delta_{c_1 c_3} \delta_{c_2 c_4} + \bar{v}_2 P_R \not{k}_3 u_1 \frac{1}{\hat{t}} \delta_{c_1 c_3} \delta_{c_2 c_4} \right]. \end{aligned} \quad (\text{A.3})$$

In these expressions, \hat{t} and \hat{u} denote usual Mandelstam variables, \bar{v}_m and u_m stand for four-component spinors associated with an initial particle of momentum k_m , P_L and P_R are left-handed and right-handed chirality projectors, and m_μ refers to the muon mass.

After averaging over the initial degrees of freedom and squaring the amplitudes, we obtain the following relation between the associated cross sections

$$\frac{\sigma[pp \rightarrow R_2^{(+5/3)} S_3^{(-1/3)}]}{\sigma[pp \rightarrow R_2^{(+2/3)} S_3^{(+2/3)}]} \approx \frac{1}{2} \left(\frac{y_{2,12}^{\text{LR}}}{y_{2,12}^{\text{RL}}} \right)^2, \quad (\text{A.4})$$

which can also be derived at the level of the amplitudes (A.3) in the limit $m_\mu \rightarrow 0$. The complex conjugate processes lead to relatively much smaller cross sections when the leptoquarks couple to up quarks, whereas they are comparable when initial quarks are charm quarks. These effects are PDF-driven.

Charge ± 1 – Three partonic processes lead to the production of a pair of leptoquarks whose total electric charge is equal to $+1$,

$$\bar{d}u \rightarrow R_2^{(-2/3)} R_2^{(+5/3)}, \quad \bar{d}u \rightarrow S_3^{(+1/3)} S_3^{(+2/3)} \quad \text{and} \quad \bar{d}u \rightarrow S_3^{(+4/3)} S_3^{(-1/3)}. \quad (\text{A.5})$$

At leading order, this proceeds through the annihilation of a down-type antiquark and an up-type quark, and the corresponding amplitudes read

$$\begin{aligned} \mathcal{M}_{R_2^{(-2/3)} R_2^{(+5/3)}} &= \left(y_{2,12}^{\text{RL}} \right)^2 \left[m_\mu \bar{v}_1 P_R u_2 + \bar{v}_1 P_R \not{k}_3 u_2 \right] \delta_{c_1 c_3} \delta_{c_2 c_4} \frac{1}{\hat{t}}, \\ \mathcal{M}_{S_3^{(+1/3)} S_3^{(+2/3)}} &= \sqrt{2} \left(y_{3,12}^{\text{LL}} \right)^2 \left[\bar{v}_1 P_R \not{k}_3 u_2 \right] \delta_{c_1 c_3} \delta_{c_2 c_4} \frac{1}{\hat{t}}, \\ \mathcal{M}_{S_3^{(+4/3)} S_3^{(-1/3)}} &= \sqrt{2} \left(y_{3,12}^{\text{LL}} \right)^2 \left[\bar{v}_1 P_R \not{k}_3 u_2 \right] \delta_{c_1 c_3} \delta_{c_2 c_4} \frac{1}{\hat{t}}. \end{aligned} \quad (\text{A.6})$$

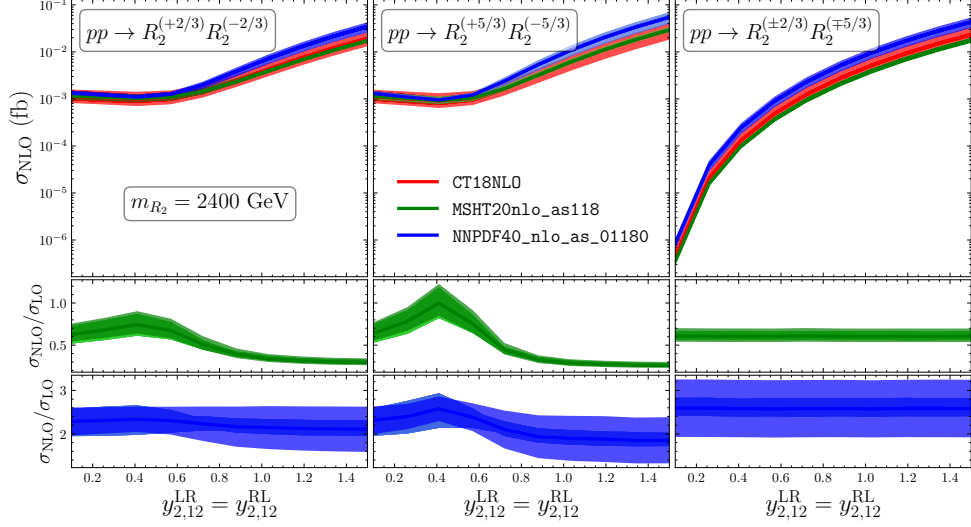


Figure 9. Same as in figure 2 but for $m_{R_2} = 2400$ GeV.

From these expressions, we derive the associated cross sections and find that they satisfy

$$\frac{\sigma\left[pp \rightarrow R_2^{(-2/3)} R_2^{(+5/3)}\right]}{\sigma\left[pp \rightarrow S_3^{(+1/3)} S_3^{(+2/3)}\right]} = \frac{\sigma\left[pp \rightarrow R_2^{(-2/3)} R_2^{(+5/3)}\right]}{\sigma\left[pp \rightarrow S_3^{(+4/3)} S_3^{(-1/3)}\right]} \approx \frac{1}{2} \left(\frac{y_{2,12}^{\text{RL}}}{y_{3,12}^{\text{LL}}} \right)^4. \quad (\text{A.7})$$

Charge $\pm 1/3$ – There are two partonic processes leading to the production of a pair of leptoquarks whose total electric charge is equal to $+1/3$,

$$ud \rightarrow R_2^{(+2/3)} S_3^{(-1/3)} \quad \text{and} \quad ud \rightarrow R_2^{(+5/3)} S_3^{(-4/3)}. \quad (\text{A.8})$$

They occur through the annihilation of an up-type and a down-type quark, and in the limit of vanishing muon mass, the corresponding Feynman amplitudes read

$$\begin{aligned} \mathcal{M}_{R_2^{(+2/3)} S_3^{(-1/3)}} &= - \left(y_{2,12}^{\text{RL}} y_{3,12}^{\text{LL}} \right) \left[\bar{v}_1 P_L \not{k}_3 u_2 \right] \delta_{c_1 c_3} \delta_{c_2 c_4} \frac{1}{\hat{t}}, \\ \mathcal{M}_{R_2^{(+5/3)} S_3^{(-4/3)}} &= \sqrt{2} \left(y_{2,12}^{\text{RL}} y_{3,12}^{\text{LL}} \right) \left[\bar{v}_1 P_L \not{k}_3 u_2 \right] \delta_{c_1 c_3} \delta_{c_2 c_4} \frac{1}{\hat{t}}. \end{aligned} \quad (\text{A.9})$$

Using the fact these two processes have the same partonic luminosities, one derive a ratio of cross sections that fulfils

$$\frac{\sigma\left[pp \rightarrow R_2^{(+2/3)} S_3^{(-1/3)}\right]}{\sigma\left[pp \rightarrow R_2^{(+5/3)} S_3^{(-4/3)}\right]} = \frac{1}{2}. \quad (\text{A.10})$$

B Additional results for $m_{\text{LQ}} = 2400$ GeV

In this section, we show predictions for leptoquark production in the R_2 - S_3 model for $m_{R_2} = m_{S_3} = 2400$ GeV. Figure 9 shows total cross sections at NLO (and the corresponding K -factors) for the processes $pp \rightarrow R_2^{(+2/3)} R_2^{(-2/3)}$, $pp \rightarrow R_2^{(+5/3)} R_2^{(-5/3)}$ and

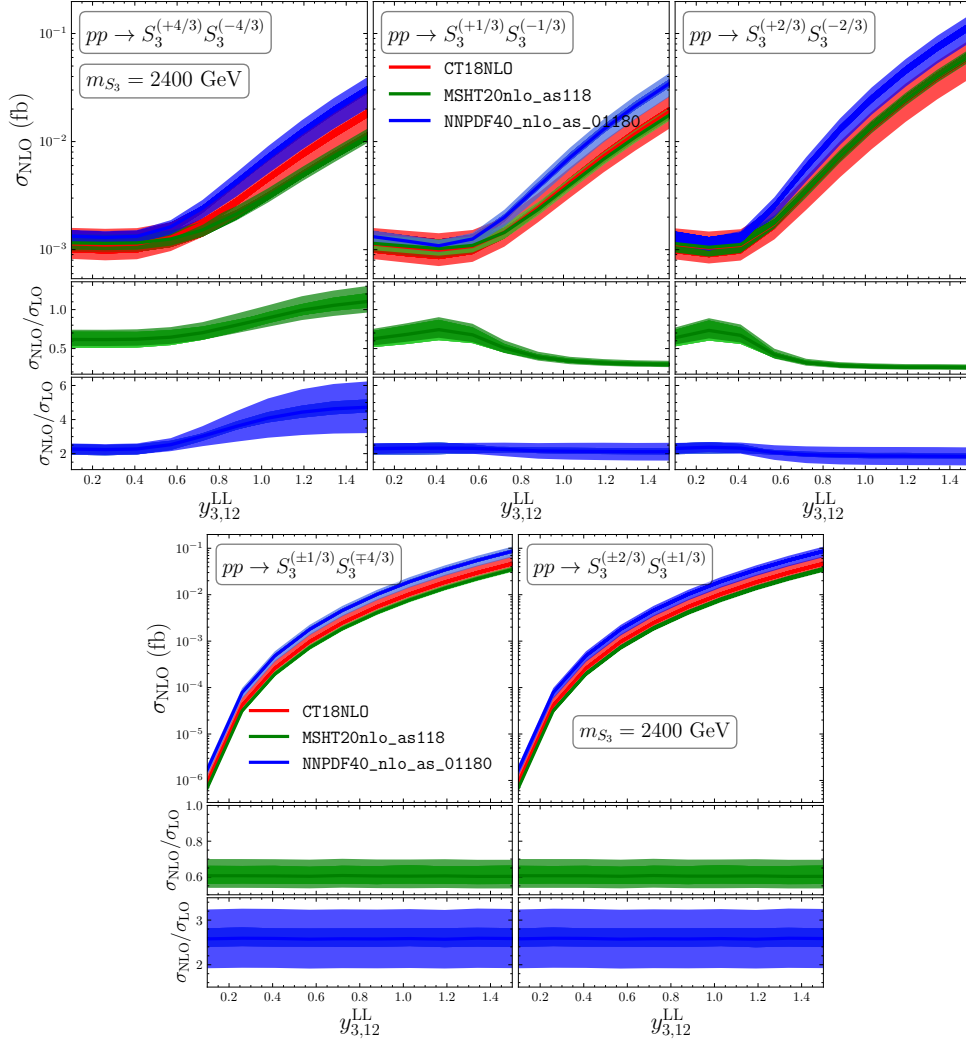


Figure 10. Same as in figure 3 but for $m_{R_2} = m_{S_3} = 2400$ GeV.

$pp \rightarrow R_2^{(\pm 5/3)} R_2^{(\mp 2/3)}$, and investigates how they depend on $y = y_{2,12}^{\text{LR}} = y_{2,12}^{\text{RL}}$. Our findings are similar as for $m_{R_2} = 1600$ GeV (see figure 4), although predictions obtained with NNPDF4.0 suffer from much larger errors. When increasing y from 0.8 to 1.5, we observe the resulting diagonal production mode cross sections to increase by almost a factor of 30, reaching about $\mathcal{O}(50)$ ab. Additionally, the off-diagonal production rate also increases by almost five orders of magnitudes, being similar to the diagonal rates for Yukawa coupling values of $y = 1.5$. Finally, whereas LO predictions depend quite a lot on the chosen PDF set (as shown with the K -factors), this dependence is reduced at NLO. Similar trends can be observed for processes involving a diagonal pair of S_3 leptoquark eigenstates in figure 10.

Results for the mixed R_2 - S_3 channels ($pp \rightarrow R_2^{(\pm 2/3)} S_3^{(\mp 1/3)}$, $pp \rightarrow R_2^{(\pm 2/3)} S_3^{(\pm 2/3)}$, $pp \rightarrow R_2^{(\pm 5/3)} S_3^{(\mp 1/3)}$, and $R_2^{(\pm 5/3)} S_3^{(\mp 4/3)}$) are shown in figure 11. As for all the off-diagonal channels, K -factors are flat and independent of the value of the y coupling. On the other

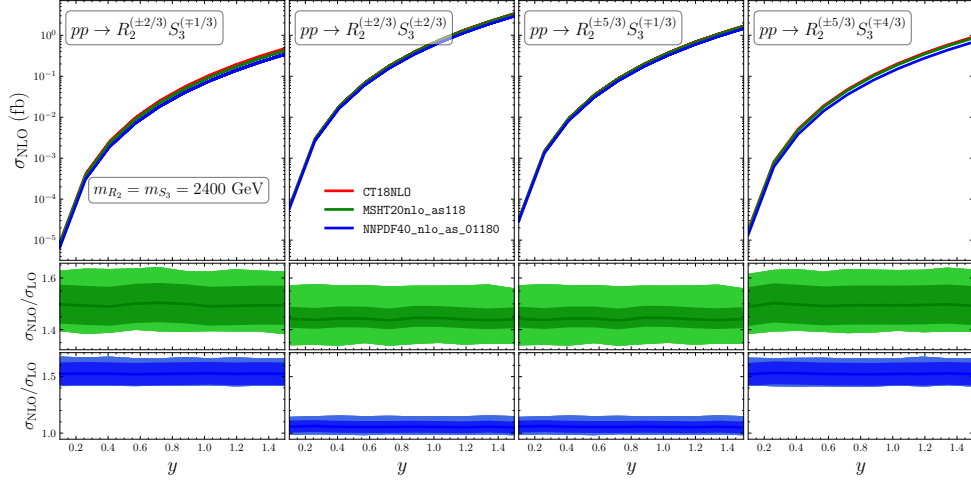


Figure 11. Same as in figure 4 but for $m_{R_2} = m_{S_3} = 2400$ GeV.

hand, the size of these K -factors are process-dependent for the NNPDF4.0 PDF set, whilst they are almost independent of the process for the MSHT20 PDF set. This can be again traced back to the poor PDF fits at LO, an effect that is fully compensated with NLO predictions. Moreover, rates for the mixed channels increase dramatically for large y values, reaching values of 1–3 fb that are relevant for the LHC for the $pp \rightarrow R_2^{(\pm 5/3)} S_3^{(\mp 4/3)}$, $pp \rightarrow R_2^{(\pm 5/3)} S_3^{(\mp 1/3)}$, and $pp \rightarrow R_2^{(\pm 2/3)} S_3^{(\pm 2/3)}$ processes.

Results illustrating the importance of the off-diagonal and t -channel contributions over the pure QCD contribution for $m_{LQ} = 2400$ GeV are reported in figures 12–14. These figures show similar findings as those described in section 3.3.

References

- [1] J. C. Pati and A. Salam, *Unified Lepton-Hadron Symmetry and a Gauge Theory of the Basic Interactions*, *Phys. Rev. D* **8** (1973) 1240–1251.
- [2] J. C. Pati and A. Salam, *Lepton Number as the Fourth Color*, *Phys. Rev. D* **10** (1974) 275–289. [Erratum: *Phys. Rev. D* 11, 703–703 (1975)].
- [3] H. Georgi and S. L. Glashow, *Unity of All Elementary Particle Forces*, *Phys. Rev. Lett.* **32** (1974) 438–441.
- [4] H. Fritzsch and P. Minkowski, *Unified Interactions of Leptons and Hadrons*, *Annals Phys.* **93** (1975) 193–266.
- [5] G. Senjanovic and A. Sokorac, *Light Leptoquarks in $SO(10)$* , *Z. Phys. C* **20** (1983) 255.
- [6] P. H. Frampton and B.-H. Lee, *$SU(15)$ GRAND UNIFICATION*, *Phys. Rev. Lett.* **64** (1990) 619.
- [7] H. Murayama and T. Yanagida, *A viable $SU(5)$ GUT with light leptoquark bosons*, *Mod. Phys. Lett. A* **7** (1992) 147–152.

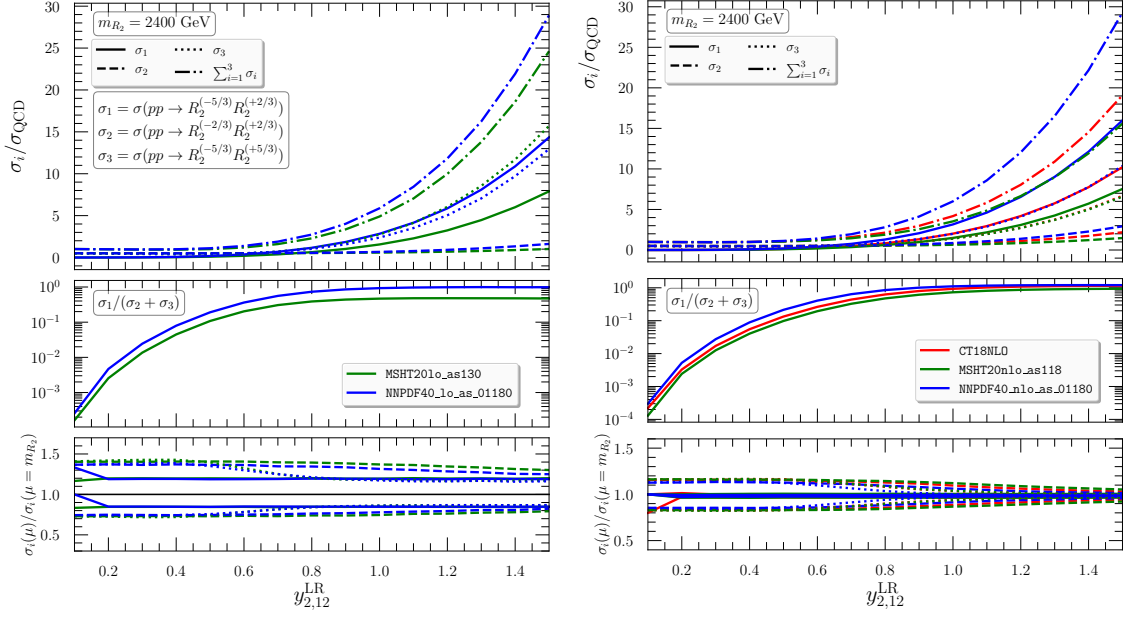


Figure 12. Same as in figure 5 but for $m_{R_2} = 2400$ GeV.

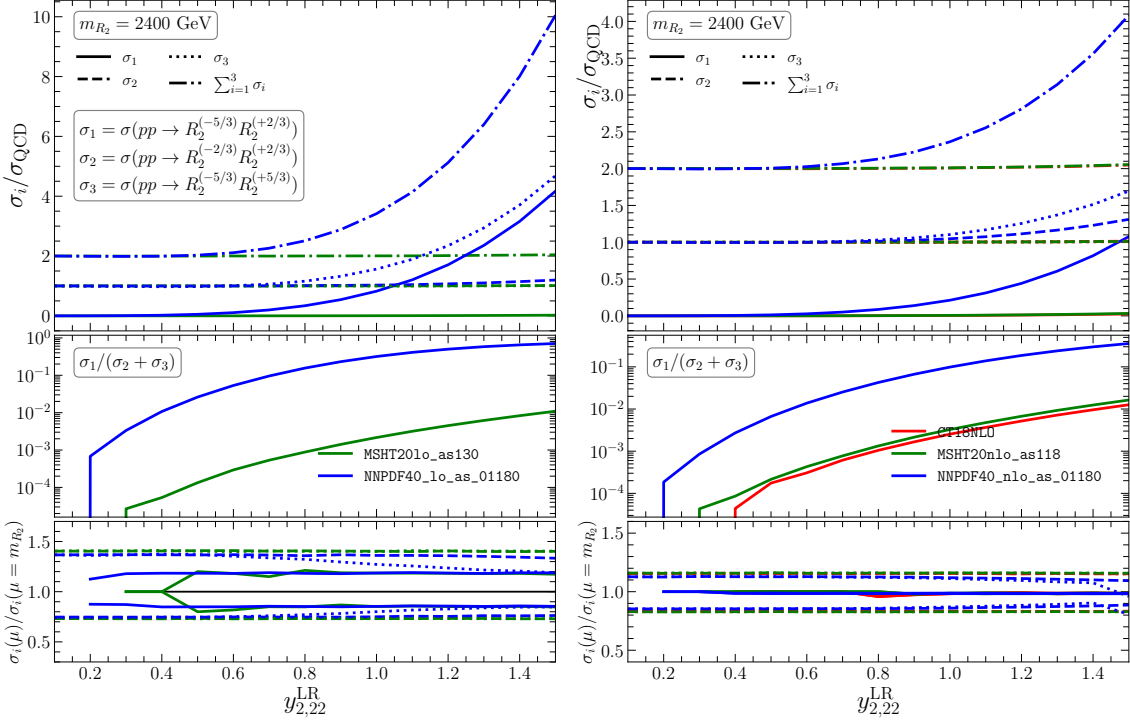


Figure 13. Same as in figure 6 but for $m_{R_2} = 2400$ GeV.

- [8] J. L. Hewett and T. G. Rizzo, *Low-Energy Phenomenology of Superstring Inspired E(6) Models*, *Phys. Rept.* **183** (1989) 193.

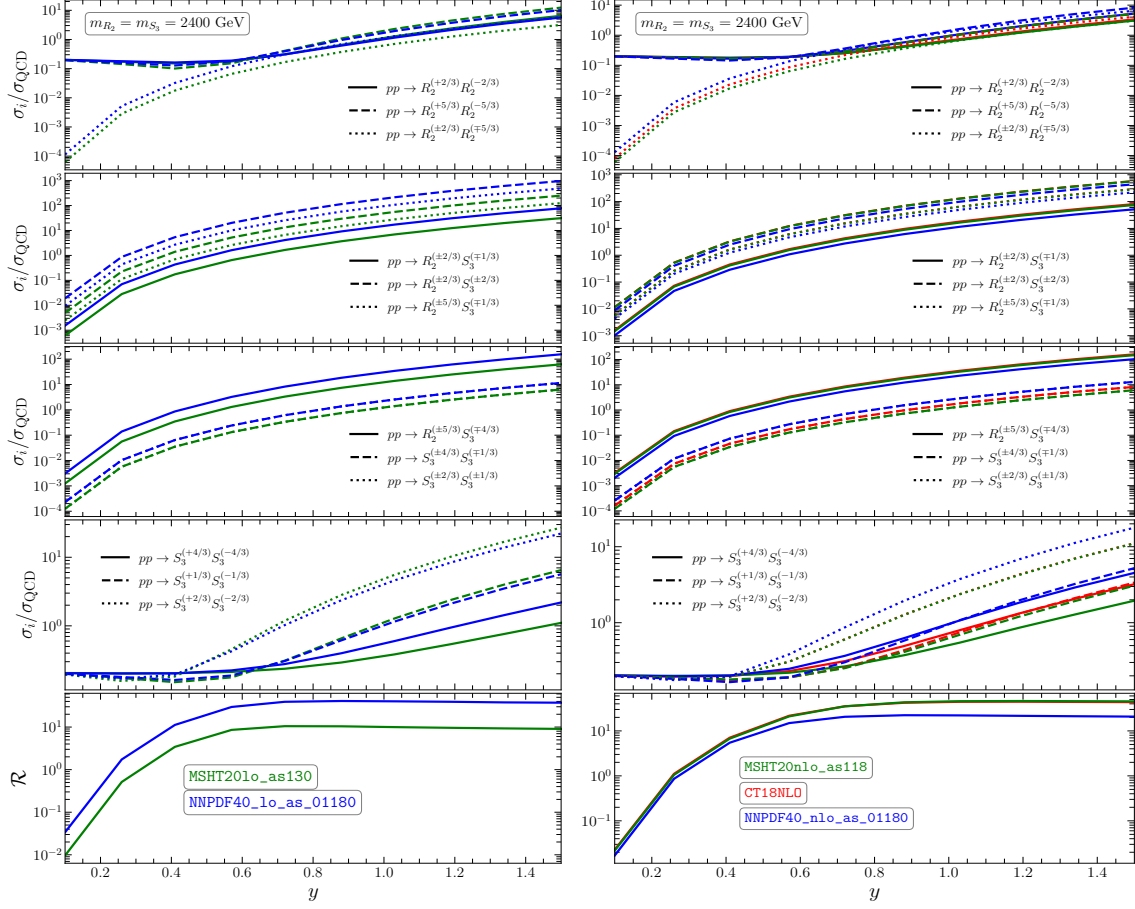


Figure 14. Same as in figure 7 but for $m_{R_2} = m_{S_3} = 2400$ GeV.

- [9] G. R. Farrar and P. Fayet, *Phenomenology of the Production, Decay, and Detection of New Hadronic States Associated with Supersymmetry*, *Phys. Lett. B* **76** (1978) 575–579.
- [10] R. Barbier et al., *R-parity violating supersymmetry*, *Phys. Rept.* **420** (2005) 1–202, [[hep-ph/0406039](#)].
- [11] S. Dimopoulos and L. Susskind, *Mass Without Scalars*, *Nucl. Phys. B* **155** (1979) 237–252.
- [12] E. Eichten and K. D. Lane, *Dynamical Breaking of Weak Interaction Symmetries*, *Phys. Lett. B* **90** (1980) 125–130.
- [13] E. Farhi and L. Susskind, *Technicolor*, *Phys. Rept.* **74** (1981) 277.
- [14] B. Schrempp and F. Schrempp, *LIGHT LEPTOQUARKS*, *Phys. Lett. B* **153** (1985) 101–107.
- [15] K. D. Lane and M. V. Ramana, *Walking technicolor signatures at hadron colliders*, *Phys. Rev. D* **44** (1991) 2678–2700.
- [16] I. Dorsner and P. Fileviez Perez, *Unification without supersymmetry: Neutrino mass, proton decay and light leptoquarks*, *Nucl. Phys. B* **723** (2005) 53–76, [[hep-ph/0504276](#)].
- [17] K. S. Babu and J. Julio, *Two-Loop Neutrino Mass Generation through Leptoquarks*, *Nucl.*

- Phys. B* **841** (2010) 130–156, [[arXiv:1006.1092](#)].
- [18] K. S. Babu, P. S. B. Dev, S. Jana, and A. Thapa, *Non-Standard Interactions in Radiative Neutrino Mass Models*, *JHEP* **03** (2020) 006, [[arXiv:1907.09498](#)].
 - [19] I. Bigaran, J. Gargalionis, and R. R. Volkas, *A near-minimal leptoquark model for reconciling flavour anomalies and generating radiative neutrino masses*, *JHEP* **10** (2019) 106, [[arXiv:1906.01870](#)].
 - [20] J. Julio, S. Saad, and A. Thapa, *A Tale of Flavor Anomalies and the Origin of Neutrino Mass*, [arXiv:2202.10479](#).
 - [21] J. Julio, S. Saad, and A. Thapa, *Marriage between neutrino mass and flavor anomalies*, [arXiv:2203.15499](#).
 - [22] M. J. Baker et al., *The Coannihilation Codex*, *JHEP* **12** (2015) 120, [[arXiv:1510.03434](#)].
 - [23] S.-M. Choi, Y.-J. Kang, H. M. Lee, and T.-G. Ro, *Lepto-Quark Portal Dark Matter*, *JHEP* **10** (2018) 104, [[arXiv:1807.06547](#)].
 - [24] D. Guadagnoli, M. Reboud, and P. Stangl, *The Dark Side of 4321* , *JHEP* **10** (2020) 084, [[arXiv:2005.10117](#)].
 - [25] G. Arcadi, L. Calibbi, M. Fedele, and F. Mescia, *Muon $g - 2$ and B -anomalies from Dark Matter*, *Phys. Rev. Lett.* **127** (2021), no. 6 061802, [[arXiv:2104.03228](#)].
 - [26] G. Belanger et al., *Leptoquark manoeuvres in the dark: a simultaneous solution of the dark matter problem and the $R_{D^{(*)}}$ anomalies*, *JHEP* **02** (2022) 042, [[arXiv:2111.08027](#)].
 - [27] M. J. Baker, D. A. Faroughy, and S. Trifinopoulos, *Collider signatures of coannihilating dark matter in light of the B -physics anomalies*, *JHEP* **11** (2021) 084, [[arXiv:2109.08689](#)].
 - [28] A. Crivellin, D. Mueller, and F. Saturnino, *Correlating $h \rightarrow \mu + \mu^-$ to the Anomalous Magnetic Moment of the Muon via Leptoquarks*, *Phys. Rev. Lett.* **127** (2021), no. 2 021801, [[arXiv:2008.02643](#)].
 - [29] A. Angelescu, D. Bećirević, D. A. Faroughy, F. Jaffredo, and O. Sumensari, *Single leptoquark solutions to the B -physics anomalies*, *Phys. Rev. D* **104** (2021), no. 5 055017, [[arXiv:2103.12504](#)].
 - [30] T. Nomura and H. Okada, *Explanations for anomalies of muon anomalous magnetic dipole moment, $b \rightarrow s \mu \mu^-$, and radiative neutrino masses in a leptoquark model*, *Phys. Rev. D* **104** (2021), no. 3 035042, [[arXiv:2104.03248](#)].
 - [31] D. Marzocca and S. Trifinopoulos, *Minimal Explanation of Flavor Anomalies: B -Meson Decays, Muon Magnetic Moment, and the Cabibbo Angle*, *Phys. Rev. Lett.* **127** (2021), no. 6 061803, [[arXiv:2104.05730](#)].
 - [32] P. Fileviez Perez, C. Murgui, and A. D. Plascencia, *Leptoquarks and matter unification: Flavor anomalies and the muon $g-2$* , *Phys. Rev. D* **104** (2021), no. 3 035041, [[arXiv:2104.11229](#)].
 - [33] C. Murgui and M. B. Wise, *Scalar leptoquarks, baryon number violation, and Pati-Salam symmetry*, *Phys. Rev. D* **104** (2021), no. 3 035017, [[arXiv:2105.14029](#)].

- [34] S. Singirala, S. Sahoo, and R. Mohanta, *Light dark matter, rare B decays with missing energy in $L\mu$ - $L\tau$ model with a scalar leptoquark*, *Phys. Rev. D* **105** (2022), no. 1 015033, [[arXiv:2106.03735](#)].
- [35] A. Crivellin, B. Fuks, and L. Schnell, *Explaining the hints for lepton flavour universality violation with three S_2 leptoquark generations*, [arXiv:2203.10111](#).
- [36] **BaBar** Collaboration, J. P. Lees et al., *Evidence for an excess of $\bar{B} \rightarrow D^{(*)}\tau^-\bar{\nu}_\tau$ decays*, *Phys. Rev. Lett.* **109** (2012) 101802, [[arXiv:1205.5442](#)].
- [37] **Belle** Collaboration, A. Abdesselam et al., *Test of Lepton-Flavor Universality in $B \rightarrow K^*\ell^+\ell^-$ Decays at Belle*, *Phys. Rev. Lett.* **126** (2021), no. 16 161801, [[arXiv:1904.02440](#)].
- [38] **BELLE** Collaboration, S. Choudhury et al., *Test of lepton flavor universality and search for lepton flavor violation in $B \rightarrow K\ell\ell$ decays*, *JHEP* **03** (2021) 105, [[arXiv:1908.01848](#)].
- [39] **Belle** Collaboration, G. Caria et al., *Measurement of $\mathcal{R}(D)$ and $\mathcal{R}(D^*)$ with a semileptonic tagging method*, *Phys. Rev. Lett.* **124** (2020), no. 16 161803, [[arXiv:1910.05864](#)].
- [40] **LHCb** Collaboration, R. Aaij et al., *Test of lepton universality with $B^0 \rightarrow K^{*0}\ell^+\ell^-$ decays*, *JHEP* **08** (2017) 055, [[arXiv:1705.05802](#)].
- [41] **LHCb** Collaboration, R. Aaij et al., *Measurement of the ratio of the $B^0 \rightarrow D^{*-}\tau^+\nu_\tau$ and $B^0 \rightarrow D^{*-}\mu^+\nu_\mu$ branching fractions using three-prong τ -lepton decays*, *Phys. Rev. Lett.* **120** (2018), no. 17 171802, [[arXiv:1708.08856](#)].
- [42] **LHCb** Collaboration, R. Aaij et al., *Search for lepton-universality violation in $B^+ \rightarrow K^+\ell^+\ell^-$ decays*, *Phys. Rev. Lett.* **122** (2019), no. 19 191801, [[arXiv:1903.09252](#)].
- [43] **LHCb** Collaboration, R. Aaij et al., *Test of lepton universality in beauty-quark decays*, *Nature Phys.* **18** (2022), no. 3 277–282, [[arXiv:2103.11769](#)].
- [44] T. Aoyama et al., *The anomalous magnetic moment of the muon in the Standard Model*, *Phys. Rept.* **887** (2020) 1–166, [[arXiv:2006.04822](#)].
- [45] **Muon g-2** Collaboration, G. W. Bennett et al., *Final Report of the Muon E821 Anomalous Magnetic Moment Measurement at BNL*, *Phys. Rev. D* **73** (2006) 072003, [[hep-ex/0602035](#)].
- [46] **Muon g-2** Collaboration, B. Abi et al., *Measurement of the Positive Muon Anomalous Magnetic Moment to 0.46 ppm*, *Phys. Rev. Lett.* **126** (2021), no. 14 141801, [[arXiv:2104.03281](#)].
- [47] **ATLAS** Collaboration, M. Aaboud et al., *Searches for third-generation scalar leptoquarks in $\sqrt{s} = 13$ TeV pp collisions with the ATLAS detector*, *JHEP* **06** (2019) 144, [[arXiv:1902.08103](#)].
- [48] **ATLAS** Collaboration, G. Aad et al., *Search for a scalar partner of the top quark in the all-hadronic $t\bar{t}$ plus missing transverse momentum final state at $\sqrt{s} = 13$ TeV with the ATLAS detector*, *Eur. Phys. J. C* **80** (2020), no. 8 737, [[arXiv:2004.14060](#)].
- [49] **ATLAS** Collaboration, G. Aad et al., *Search for pairs of scalar leptoquarks decaying into quarks and electrons or muons in $\sqrt{s} = 13$ TeV pp collisions with the ATLAS detector*, *JHEP* **10** (2020) 112, [[arXiv:2006.05872](#)].

- [50] **ATLAS** Collaboration, G. Aad et al., *Search for pair production of third-generation scalar leptoquarks decaying into a top quark and a τ -lepton in pp collisions at $\sqrt{s} = 13$ TeV with the ATLAS detector*, *JHEP* **06** (2021) 179, [[arXiv:2101.11582](#)].
- [51] **ATLAS** Collaboration, G. Aad et al., *Search for new phenomena in final states with b-jets and missing transverse momentum in $\sqrt{s} = 13$ TeV pp collisions with the ATLAS detector*, *JHEP* **05** (2021) 093, [[arXiv:2101.12527](#)].
- [52] **CMS** Collaboration, A. M. Sirunyan et al., *Search for a singly produced third-generation scalar leptoquark decaying to a τ lepton and a bottom quark in proton-proton collisions at $\sqrt{s} = 13$ TeV*, *JHEP* **07** (2018) 115, [[arXiv:1806.03472](#)].
- [53] **CMS** Collaboration, A. M. Sirunyan et al., *Search for heavy neutrinos and third-generation leptoquarks in hadronic states of two τ leptons and two jets in proton-proton collisions at $\sqrt{s} = 13$ TeV*, *JHEP* **03** (2019) 170, [[arXiv:1811.00806](#)].
- [54] **CMS** Collaboration, A. M. Sirunyan et al., *Search for singly and pair-produced leptoquarks coupling to third-generation fermions in proton-proton collisions at $s=13$ TeV*, *Phys. Lett. B* **819** (2021) 136446, [[arXiv:2012.04178](#)].
- [55] M. Kramer, T. Plehn, M. Spira, and P. M. Zerwas, *Pair production of scalar leptoquarks at the Tevatron*, *Phys. Rev. Lett.* **79** (1997) 341–344, [[hep-ph/9704322](#)].
- [56] M. Kramer, T. Plehn, M. Spira, and P. M. Zerwas, *Pair production of scalar leptoquarks at the CERN LHC*, *Phys. Rev. D* **71** (2005) 057503, [[hep-ph/0411038](#)].
- [57] I. Doršner and A. Greljo, *Leptoquark toolbox for precision collider studies*, *JHEP* **05** (2018) 126, [[arXiv:1801.07641](#)].
- [58] T. Mandal, S. Mitra, and S. Seth, *Pair Production of Scalar Leptoquarks at the LHC to NLO Parton Shower Accuracy*, *Phys. Rev. D* **93** (2016), no. 3 035018, [[arXiv:1506.07369](#)].
- [59] C. Borschensky, B. Fuks, A. Kulesza, and D. Schwartländer, *Scalar leptoquark pair production at hadron colliders*, *Phys. Rev. D* **101** (2020), no. 11 115017, [[arXiv:2002.08971](#)].
- [60] C. Borschensky, B. Fuks, A. Kulesza, and D. Schwartländer, *Scalar leptoquark pair production at the LHC: precision predictions in the era of flavour anomalies*, *JHEP* **02** (2022) 157, [[arXiv:2108.11404](#)].
- [61] C. Borschensky, B. Fuks, A. Kulesza, and D. Schwartländer, *Precision predictions for scalar leptoquark pair production at the LHC*, *PoS EPS-HEP2021* (2022) 637, [[arXiv:2110.15324](#)].
- [62] A. Alves, O. Eboli, and T. Plehn, *Stop lepton associated production at hadron colliders*, *Phys. Lett. B* **558** (2003) 165–172, [[hep-ph/0211441](#)].
- [63] I. Doršner, S. Fajfer, and A. Greljo, *Cornering Scalar Leptoquarks at LHC*, *JHEP* **10** (2014) 154, [[arXiv:1406.4831](#)].
- [64] J. B. Hammett and D. A. Ross, *NLO Leptoquark Production and Decay: The Narrow-Width Approximation and Beyond*, *JHEP* **07** (2015) 148, [[arXiv:1501.06719](#)].
- [65] T. Mandal, S. Mitra, and S. Seth, *Single Productions of Colored Particles at the LHC: An Example with Scalar Leptoquarks*, *JHEP* **07** (2015) 028, [[arXiv:1503.04689](#)].

- [66] D. A. Faroughy, A. Greljo, and J. F. Kamenik, *Confronting lepton flavor universality violation in B decays with high- p_T tau lepton searches at LHC*, *Phys. Lett. B* **764** (2017) 126–134, [[arXiv:1609.07138](#)].
- [67] N. Raj, *Anticipating nonresonant new physics in dilepton angular spectra at the LHC*, *Phys. Rev. D* **95** (2017), no. 1 015011, [[arXiv:1610.03795](#)].
- [68] A. Greljo and D. Marzocca, *High- p_T dilepton tails and flavor physics*, *Eur. Phys. J. C* **77** (2017), no. 8 548, [[arXiv:1704.09015](#)].
- [69] S. Bansal, R. M. Capdevilla, A. Delgado, C. Kolda, A. Martin, and N. Raj, *Hunting leptoquarks in monolepton searches*, *Phys. Rev. D* **98** (2018), no. 1 015037, [[arXiv:1806.02370](#)].
- [70] M. Schmaltz and Y.-M. Zhong, *The leptoquark Hunter’s guide: large coupling*, *JHEP* **01** (2019) 132, [[arXiv:1810.10017](#)].
- [71] J. Fuentes-Martin, A. Greljo, J. Martin Camalich, and J. D. Ruiz-Alvarez, *Charm physics confronts high- p_T lepton tails*, *JHEP* **11** (2020) 080, [[arXiv:2003.12421](#)].
- [72] U. Haisch, L. Schnell, and S. Schulte, *On Drell-Yan production of scalar leptoquarks coupling to heavy-quark flavours*, [arXiv:2207.00356](#).
- [73] J. Ohnemus, S. Rudaz, T. F. Walsh, and P. M. Zerwas, *Single leptoquark production at hadron colliders*, *Phys. Lett. B* **334** (1994) 203–207, [[hep-ph/9406235](#)].
- [74] O. J. P. Eboli, R. Zukanovich Funchal, and T. L. Lungov, *Signal and backgrounds for leptoquarks at the CERN LHC*, *Phys. Rev. D* **57** (1998) 1715–1729, [[hep-ph/9709319](#)].
- [75] L. Buonocore, U. Haisch, P. Nason, F. Tramontano, and G. Zanderighi, *Lepton-Quark Collisions at the Large Hadron Collider*, *Phys. Rev. Lett.* **125** (2020), no. 23 231804, [[arXiv:2005.06475](#)].
- [76] A. Greljo and N. Selimovic, *Lepton-Quark Fusion at Hadron Colliders, precisely*, *JHEP* **03** (2021) 279, [[arXiv:2012.02092](#)].
- [77] I. Doršner, S. Fajfer, and A. Lejlić, *Novel Leptoquark Pair Production at LHC*, *JHEP* **05** (2021) 167, [[arXiv:2103.11702](#)].
- [78] J. Alwall, R. Frederix, S. Frixione, V. Hirschi, F. Maltoni, O. Mattelaer, H. S. Shao, T. Stelzer, P. Torrielli, and M. Zaro, *The automated computation of tree-level and next-to-leading order differential cross sections, and their matching to parton shower simulations*, *JHEP* **07** (2014) 079, [[arXiv:1405.0301](#)].
- [79] P. Nason, *A New method for combining NLO QCD with shower Monte Carlo algorithms*, *JHEP* **11** (2004) 040, [[hep-ph/0409146](#)].
- [80] S. Frixione, P. Nason, and C. Oleari, *Matching NLO QCD computations with Parton Shower simulations: the POWHEG method*, *JHEP* **11** (2007) 070, [[arXiv:0709.2092](#)].
- [81] S. Alioli, P. Nason, C. Oleari, and E. Re, *A general framework for implementing NLO calculations in shower Monte Carlo programs: the POWHEG BOX*, *JHEP* **06** (2010) 043, [[arXiv:1002.2581](#)].

- [82] W. Buchmuller, R. Ruckl, and D. Wyler, *Leptoquarks in Lepton - Quark Collisions*, *Phys. Lett. B* **191** (1987) 442–448. [Erratum: *Phys.Lett.B* 448, 320–320 (1999)].
- [83] I. Doršner, S. Fajfer, A. Greljo, J. F. Kamenik, and N. Košnik, *Physics of leptoquarks in precision experiments and at particle colliders*, *Phys. Rept.* **641** (2016) 1–68, [[arXiv:1603.04993](#)].
- [84] A. Crivellin and L. Schnell, *Complete Lagrangian and set of Feynman rules for scalar leptoquarks*, *Comput. Phys. Commun.* **271** (2022) 108188, [[arXiv:2105.04844](#)].
- [85] O. Popov, M. A. Schmidt, and G. White, *R_2 as a single leptoquark solution to $R_{D^{(*)}}$ and $R_{K^{(*)}}$* , *Phys. Rev. D* **100** (2019), no. 3 035028, [[arXiv:1905.06339](#)].
- [86] D. Bečirević, I. Doršner, S. Fajfer, N. Košnik, D. A. Faroughy, and O. Sumensari, *Scalar leptoquarks from grand unified theories to accommodate the B -physics anomalies*, *Phys. Rev. D* **98** (2018), no. 5 055003, [[arXiv:1806.05689](#)].
- [87] D. Bečirević, F. Jaffredo, A. Peñuelas, and O. Sumensari, *New Physics effects in leptonic and semileptonic decays*, *JHEP* **05** (2021) 175, [[arXiv:2012.09872](#)].
- [88] A. Crivellin, D. Müller, and F. Saturnino, *Flavor Phenomenology of the Leptoquark Singlet-Triplet Model*, *JHEP* **06** (2020) 020, [[arXiv:1912.04224](#)].
- [89] C. Degrande, C. Duhr, B. Fuks, D. Grellscheid, O. Mattelaer, and T. Reiter, *UFO - The Universal FeynRules Output*, *Comput. Phys. Commun.* **183** (2012) 1201–1214, [[arXiv:1108.2040](#)].
- [90] A. Buckley, J. Ferrando, S. Lloyd, K. Nordström, B. Page, M. Rüfenacht, M. Schönherr, and G. Watt, *LHAPDF6: parton density access in the LHC precision era*, *Eur. Phys. J. C* **75** (2015) 132, [[arXiv:1412.7420](#)].
- [91] S. Bailey, T. Cridge, L. A. Harland-Lang, A. D. Martin, and R. S. Thorne, *Parton distributions from LHC, HERA, Tevatron and fixed target data: MSHT20 PDFs*, *Eur. Phys. J. C* **81** (2021), no. 4 341, [[arXiv:2012.04684](#)].
- [92] R. D. Ball et al., *The Path to Proton Structure at One-Percent Accuracy*, [arXiv:2109.02653](#).
- [93] T.-J. Hou et al., *New CTEQ global analysis of quantum chromodynamics with high-precision data from the LHC*, *Phys. Rev. D* **103** (2021), no. 1 014013, [[arXiv:1912.10053](#)].
- [94] T. Hahn, *Generating Feynman diagrams and amplitudes with FeynArts 3*, *Comput. Phys. Commun.* **140** (2001) 418–431, [[hep-ph/0012260](#)].
- [95] T. Hahn and M. Perez-Victoria, *Automatized one loop calculations in four-dimensions and D -dimensions*, *Comput. Phys. Commun.* **118** (1999) 153–165, [[hep-ph/9807565](#)].